buildings

Review

The Soil-Arching Effect in Pile-Supported Embankments: A Review

Kangyu Wang [1,2], Jiahuan Ye [1], Xinquan Wang [3,4,5,*] and Ziliang Qiu [1]

[1] School of Civil Engineering, Zhejiang University of Technology, Hangzhou 310014, China; kangyuwang@zjut.edu.cn (K.W.); 211122060039@zjut.edu.cn (J.Y.); qzl5579@163.com (Z.Q.)
[2] Zhejiang Key Laboratory of Civil Engineering Structures & Disaster Prevention and Mitigation Technology, Hangzhou 310014, China
[3] Department of Civil Engineering, Hangzhou City University, Hangzhou 310015, China
[4] Key Laboratory of Safe Construction and Intelligent Maintenance for Urban Shield Tunnels of Zhejiang Province, Hangzhou 310015, China
[5] Zhejiang Engineering Research Center of Intelligent Urban Infrastructure, Hangzhou 310015, China
* Correspondence: wangxq@hzcu.edu.cn

Abstract: Pile-supported embankments are widely used in foundation treatments, owing to their safety, efficient construction, and economy. The soil-arching effect is a key load-transferring mechanism in a pile-supported embankment, and it reduces the even settlement on the embankment surface. In recent years, researchers and engineers have conducted extensive research on the soil-arching phenomenon in pile-supported embankments. This paper reviews relevant studies on the effect of soil arching in pile-supported embankments in order to better understand the mechanism and influencing factors of the distribution of the arching effect. First, the development history of the practice and theory related to pile-supported embankments is discussed. This is followed by a review of theoretical studies on the soil-arching effect, load distribution and soil deformation on pile-supported embankments (with and without geogrid reinforcement), and structures and factors influencing soil arching. The results of these studies are summarized, and finally, topics for future research are suggested, providing references for the design and maintenance of civil infrastructure.

Keywords: pile-supported embankment; soil arching; load distribution; deformation; factors

Citation: Wang, K.; Ye, J.; Wang, X.; Qiu, Z. The Soil-Arching Effect in Pile-Supported Embankments: A Review. *Buildings* **2024**, *14*, 126. https://doi.org/10.3390/buildings14010126

Academic Editor: Yong Tan

Received: 27 November 2023
Revised: 26 December 2023
Accepted: 2 January 2024
Published: 3 January 2024

1. Introduction

The construction of civil engineering infrastructure is often associated with the low strength and high compressibility of the soil, which is not conducive to engineering construction. Problems, such as the failure of foundation-bearing capacity, excessive differential settlement and total settlement, and subgrade slope failure, are frequently encountered in civil engineering due to the above conditions. To deal with these problems, preloading methods [1], drainage consolidation [2], substitution method, and dynamic compaction [3] have been widely used to improve soft soil. However, these methods have disadvantages, such as long construction periods and significant foundation settlement, which is difficult to control after completing the construction. Therefore, these methods are inapplicable in complex construction environments under varying working conditions. To adapt to the increasingly complex construction conditions and meet the demand for rapid embankment filling, several researchers proposed the use of pile-supported embankments consisting of piles, sand–gravel cushions, and embankment filling [4–6]. Among them, the embankment filling is the main body of the embankment which can bear the embankment load and reduce the settlement of the pavement. The piles in soft soil foundations can reduce the settlement of the embankment by transferring the load in the embankment to the pile foundation through shearing and arching effects. The sand–gravel cushion, on the other hand, can avoid damage to the embankment due to the punching and cutting effects of piles.

Nowadays, the geosynthetics are also used in pile-supported embankments to decrease the lateral displacement of the soil and increase the stability of the embankment.

This paper reviews the methods and results of research conducted on pile-supported embankments in the past thirty years, including studies on the soil-arching effect, which is widely observed in such embankments. The review is aimed at better understanding the mechanism and influencing factors of the load distribution in pile-supported embankments. First, the development history of the practice and theory related to pile-supported embankments is discussed. Subsequently, we focus on theoretical research on the soil-arching effect, including the arch structure and factors influencing the arching phenomenon. Finally, topics for future research are suggested to bring about improvements in the construction of civil infrastructure.

1.1. The Application History of Pile-Supported Embankments

The use of pile foundations can be traced back to an ancient Chilean civilization 12,000 years ago. In China, pile foundations were seen 7000 years ago, according to excavations conducted in the Hemudu site, Zhejiang. Wooden piles were used in the earliest pile foundations, mainly to support the main structure of ancient houses. With the development of science and technology, the materials used in pile foundations have changed from wooden to steel, cement, concrete, and reinforced concrete. The application field has also been extended from the initial support structure of housing construction to infrastructure such as cofferdams, bridges, docks, and subgrades. Thus, pile foundations have become one of the most common foundation treatment technologies.

In 1898, the Russian engineer, Strauss, proposed the application of concrete or reinforced concrete materials in pile construction. In 1901, the American engineer, Raymond, independently put forward a design concept of an immersed tube cast-in-place pile. Since the beginning of the twentieth century, steel and concrete piles have been widely used in foundation treatment. In 1930, Buisman proposed the conventional pile-supported (CPS) embankment for a peat layer (see Figure 1), constructed with a concrete slab on timber piles, which were installed upside down to generate sufficient bearing capacity [7].

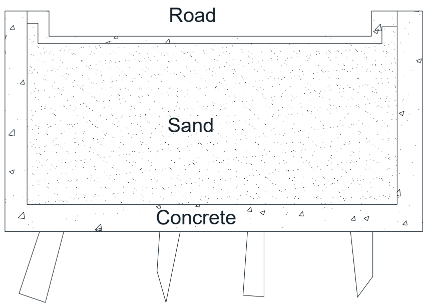

Figure 1. Early application of pile-supported embankments.

In 1951, during the construction of the river-crossing bridge over St Edmunds-Mildenhall Road (A.1101) in Berry, West Suffolk, England, a pile-supported embankment was used as the approach embankment of the bridge to improve the bearing capacity and durability of the embankment and reduce the differential settlement of the road surface [8]. The original section of Bloomington Road (1951) in Canada was expanded by a geogrid-reinforced and pile-supported (GRPS) embankment (see Figure 2) [9,10]. The results of field measurements and numerical simulations have shown that a reinforced embankment is beneficial for limiting the lateral displacement of the soil and increasing the stability of the roadbed; however, compared to the effect of limiting the lateral displacement, its effect on the consolidation settlement of the soil is not significant. Actually, although the vertical stress does not directly act on the geogrid reinforcement located between the pile caps, it can be transferred towards to the pile caps through the tense of geogrid-reinforcement. And then, the geogrid reinforcement can decrease the total settlement of subsoil and even the settlement between the pile caps, which will also influence the development of soil arching. As a result, it is meaningful and necessary to investigate the soil-arching effect and the membranate effect in the GRPS embankment.

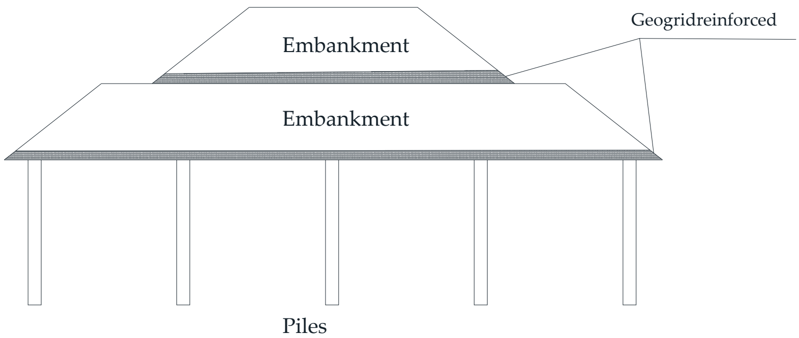

Figure 2. GRPS embankment.

1.2. The Development History of Pile-Supported Embankments

Terzaghi [11,12] established trapdoor experiments based on a CPS embankment, proposed the concept of the soil-arching effect, and discussed the distribution of the pile–soil stress under different conditions. Hewlett and Randolph [13] conducted a small-scale model experiment using dry sand based on the M9 and M876 highway approach embankment project near Glasgow [14]. Based on the experimental results, it was concluded that under 2D conditions, a soil-arching structure exhibits a semicircular shape with equal thickness, whereas it exhibits a semi-spherical shell shape with equal thickness under 3D conditions. Kempfert et al. [15,16] revised Hewlett and Randolph's soil-arching model [13] and proposed a new model composed of several semicircles. Carlson [17] and Guido et al. [18], respectively, proposed the wedge-shaped soil-arching theory and the triangular-shaped soil-arching theory to simplify the calculation models of 2D and 3D soil-arching effects.

The aforementioned theoretical models can effectively predict the stress distribution pattern in the soil and the development pattern of soil arches formed in CPS embankments. However, due to the lack of consideration for the influence of reinforcement, the theoretical calculation results obtained for GRPS embankments are not entirely consistent with the measurement results [19–21]. To completely consider the effect of reinforcement in GRPS embankments, the British Standards Institution has put forth design specifications for soil-reinforcement technology in GRPS embankments (BS8006) [22], which was updated to BS8006-1 in 2010 [23]. Germany [24], the Netherlands [25], and the United States [26] have also established relevant specifications for the design of GRPS embankments.

2. Loading Distribution and Settlement

2.1. The Definition of Soil-Arching Effect

Soil arching is one of the most common phenomena encountered in geotechnical engineering applications, such as in tunnels, buried piles, and pile-supported embankments [11,12]. In fact, the soil-arching effect is a mechanical phenomenon wherein pressure is transferred from a yielding mass of soil to the adjoining stationary part. As shown in Figure 3, when a mass of soil yields while the rest remains intact, a shearing resistance will occur between the yielding soil and the stationary mass (i.e., lines ac and bd). This shearing resistance reduces the pressure within the yielding zone while the pressure within the adjoining soil increases. In other words, the pressure within the yielding part of the mass is transferred to the adjoining part due to the shearing resistance.

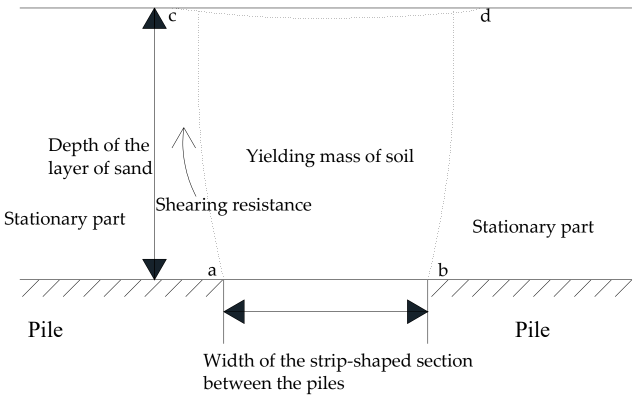

Figure 3. The mechanization of soil arching.

Unfortunately, Terzaghi did not describe the shape of the soil arch. To further study the soil-arching phenomenon, based on Terzaghi's method, Handy [27] proposed the concept of minor principal stress arching. In this method, the soil-arching model is composed of two parallel, unyielding, rough vertical walls, and granular filling. With the minor circle method, the soil arch can be described as a continuous and compressing arch that dips downward instead of upward if the arch is supportive, and the shape of arch should dip upward if the reverse is true. Kellogg [28] discussed Handy's method and pointed out some limitations. Carlson [17] proposed the wedge-shaped soil-arching theory, which is applied by the Japanese Design Manual [29] and Nordic Design Guidelines [30]. Guido [18] proposed the triangular-shaped soil-arching theory, which simplifies the calculation method for soil arching.

Hewlett and Randolph [13] proposed soil arch models with 2D equal-thickness semi-circular and 3D equal-thickness shell shapes (as shown in Figure 4a); the models were used in further research on the soil-arching effect. These models are discussed in Section 2.2.2.

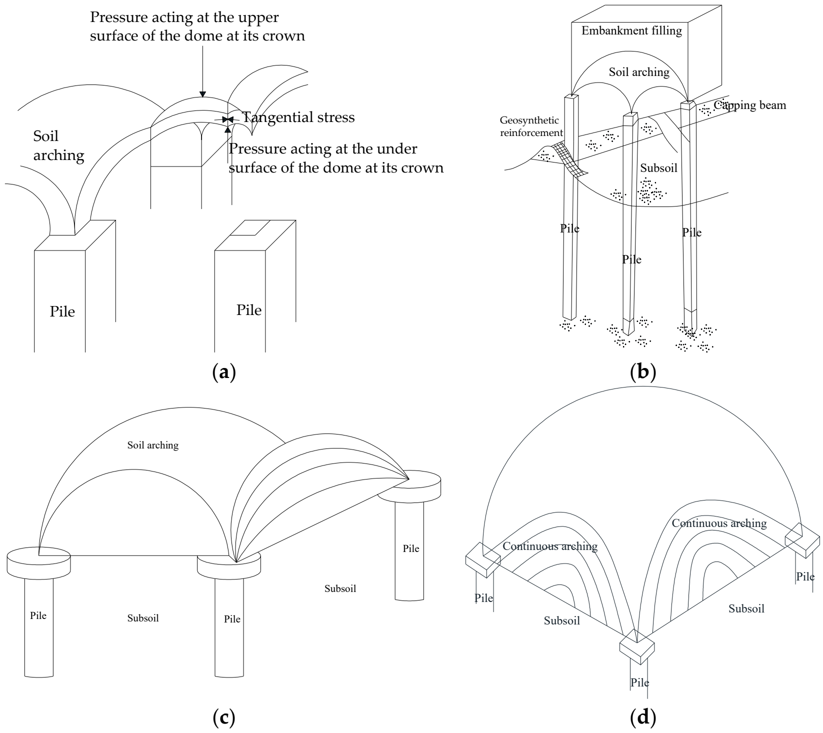

Figure 4. Soil aching model. (**a**) Hewlett and Randolph's equal-thickness shell soil-arch model.

(**b**) Low's soil-arching model of embankment piles with cap beam and geotextile. (**c**) Zaeske's multi-scale model [31]. (**d**) The Concentric Arches model.

However, the above method ignores the function of the geosynthetic reinforcement, because of which the calculation results are not entirely consistent with the field measurement results. Based on Hewlett and Randolph's model (as shown in Figure 4a), Low et al. [21] considered the effect of geosynthetic reinforcement and improved the model (as shown in Figure 4b) and the calculation of the soil arching. A multiscale model (as shown in Figure 4c) was proposed by Zaeske and described by Kempfert [31]; it is adopted in EBGEO [24]. Combining Hewlett and Randolph's model and Zaeske's multiscale model, Van Eekelen et al. [32,33] proposed a concentric-arching model, as shown in Figure 4d.

Soil arching is influenced by many factors, including the pile shape, embankment-filling parameters, and subsoil and geosynthetic reinforcement (stiffness, arrangement pattern, and material characteristics). These factors are discussed in Section 3.

2.2. Different Calculation Methods for Load Distribution

Numerous calculation models have been proposed to understand the transfer characteristics between piles and subsoil, such as the trapdoor model [12], triangular arching model [17], hemispherical model [13], and semicircular model [21]. Based on these models and models that were extended from these, the load distribution between the pile and subsoil can be classified into two types. The first one is based on the trapdoor model and the other one is based on the hemispherical model or its extended models.

2.2.1. Load Distribution Based on the Trapdoor Model

As shown in Figure 5, the vertical pressure along the horizontal axis is assumed to be uniformly distributed, and the sliding plates are assumed to be vertical planes. The soil between the supports is divided into units, the thickness of which can be considered infinitesimal, and the thickness of a unit can be represented by dz. The weight of the unit is defined as $2L\gamma dz$, and the weight of the overlying soil is $2L\gamma z$, where $2L$ is the width of the sliding plates, and γ is the unit weight of the soil. Assuming that the vertical stress at any depth into the soil is σ_{v}, the vertical stress below the unit will be $\sigma_{\mathrm{v}} + d\sigma_{\mathrm{v}}$. If there is a slippage or a trend of slippage, a shearing resistance will occur between the soil and the support structure, defined as $c + \sigma_{\mathrm{k}}\tan\varphi$, where c is the cohesion of the soil and σ_{k} is the horizontal stress acting on the soil. Clearly, the numbers of the increased vertical stress at the support structure and the decreased vertical stress at the yielding soil are both equal to $c + \sigma_{\mathrm{k}}\tan\varphi$. In other words, there is a stress-transfer phenomenon between the yielding soil and the support structure, whose number is equal to $c + \sigma_{\mathrm{k}}\tan\varphi$.

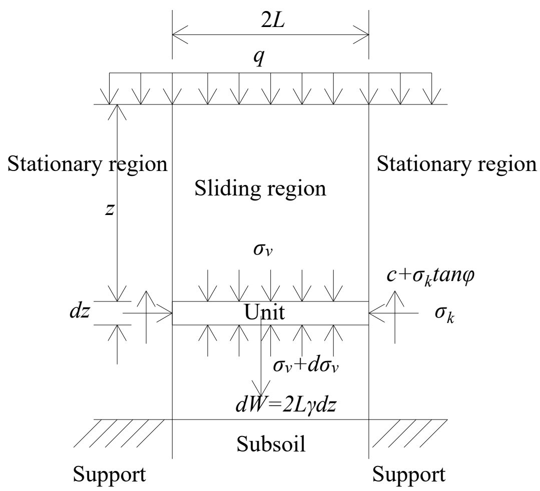

Figure 5. Diagram illustrating assumptions on which computation of pressure in sand between two vertical surfaces of sliding is based.

In the last few decades, several studies [34–37] have been conducted on soil arching or load distribution using trapdoor models. Different development patterns of arching have been observed with increasing height of the embankment fill; these patterns are discussed in Section 2.3.3. Wang et al. [38] also set up a trapdoor physical model considering a geogrid and discussed the stress distribution on a pile-supported embankment. And, there are five kinds of models (which have different sizes of pile cap or vary in the number of geogrid sheets used in which the same phenomena can be observed: an increase in the pressure above the pile cap with decreasing embankment height. However, there is a special range where the soil pressure above the pile cap increases faster while the pressure above the surface between the pile caps decreases. The soil pressure above the pile cap is greater than that above the subsurface between the caps, indicating a pressure transfer from the subsurface to the pile cap due to the soil-arching effect. Evidently, the pressure transfer effect fades away outside the reference range. The special range in which there is a phenomenon of pressure transfer is considered to correspond to the presence of soil arching, which will also be discussed in Section 2.3.3.

The load distribution between the pile cap and the subsurface under the soil-arching effect can be better understood through the trapdoor model. However, the aforementioned method is associated with limitations: it ignores many factors influencing the stress transfer, because of which the obtained results do not completely match the practically observed phenomenon. The details of the factors influencing the stress transfer and soil arching will be discussed in Section 3.

Many investigations on the arching phenomenon [39–41] have been conducted using a one-segment rigid trapdoor model; the limitation here is that it cannot simulate the nonuniform settlement of the subsoil during fill placement and localized surface loading. To overcome this limitation, Mahdi Al-Naddaf et al. [42,43] set up a spring-based trapdoor model, which was supported by compression springs to allow for continuous displacement during fill placement and localized surface loading, thus better simulating the condition of soft subsoil in pile-supported embankments. In the test, there was degradation in the soil arching, first at the center above the trapdoor and thereafter extended to the entire area around the trapdoor, whereas in the conventional trapdoor test, a more rapid degradation was observed.

Other investigations on soil arching involving trapdoor models have also shown that the soil arch exhibits many different states during embankment construction. The development pattern of soil arches in pile-supported embankments is discussed in Section 2.3.3.

2.2.2. A Calculation Method for Load Distribution Based on Hemispherical or Its Extended Models

A semicircular or hemispherical model [13] is widely used in current studies on pile-supported embankments [21,44–49]. Clearly, the weight of an embankment fill is borne by the piles and subsoil.

To understand the load distribution pattern on a pile-supported embankment, Van Eekelen [32] proposed a concentric-arching (CA) model based on the hemispherical and multiscale models. As shown in Figure 6, a part of the total load (referred to as load part A) is transferred to the pile due to soil arching, and the rest (referred to as part B + C) is directly borne by the subsoil (in the absence of a reinforcement). However, for a GRPS embankment, the residual load is further distributed as the part that is transferred to the piles through the reinforcement (referred to as load part B) and as the part which is borne by the subsoil (referred to as load part C) [33], as shown in Figure 7. Compared with the aforementioned analytical model, it is found that the former model ignores the effect of reinforcement, while the membrane and soil-arching effects are both considered in the latter model. Therefore, the evaluation results based on the latter model may be more accurate, and the scope of application may be wider.

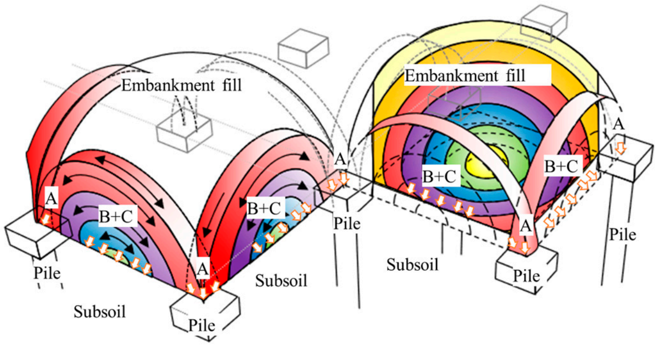

Figure 6. Three-dimensional version of the Concentric Arches (CA) model.

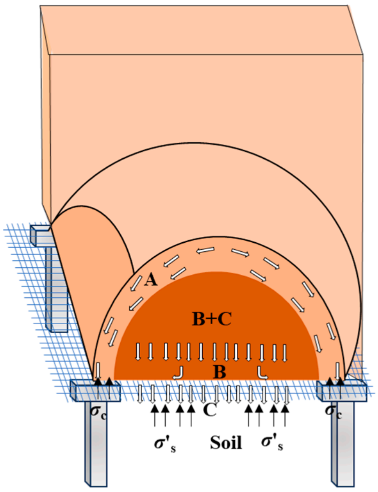

Figure 7. Definitions of load distribution in a GRPS embankment.

Figure 7 illustrates that a part of total load (load part A) is transferred to the pile cap when the soil arching occurs, which leads the piles to be subjected to a greater load. Obviously, the phenomenon of stress concentration always accompanies the soil arching, in which the concentration ratio *n* (defined as the ratio of the average stress $\sigma_s{}'$ on the pile cap and uniform stress σ_c on the subsoil) is used to describe the condition of the stress concentration in the embankment. And, in current research of soil arching, the stress reduction ratio (*SRR*), described as the ratio of the average vertical stress remaining to be carried by the subsoil after arching has occurred to the nominal vertical stress due to the embankment fill, was used to define the soil-arching degree as another important index. Obviously, the value of the *SRR* ranges from 0 to 1. If the *SRR* equals zero, it represents that all the embankment load transfers to pile caps. When *SRR* equals one, the embankment load will not be transferred, and there will be no soil arching or stress concentration.

In addition to the aforementioned soil arching indices, the efficacy *E* of the pile support, which is defined as the proportion of embankment weight carried by the piles, was proposed by Hewlett and Randolph to discuss the load distribution in a pile-supported embankments and evaluate the effect of soil arching and reinforcement. However, due to the different assumptions and analytical models used, there are different calculation methods for *E*. For example, the load part A versus the remainder part C (soil-arching effect) or the load supported by pile A + B versus the subsoil load C (arching + membrane effect) is used in the load distribution analysis of pile-supported embankments. The efficacy *E* of the pile support is equal to the load borne by the pile to the total weight of the embankment fill. And, there is also the settlement efficacy to evaluate the effect of soil arching; the details will be introduced in Section 2.3.2.

Tables 1 and 2 present different calculation equations for the efficacy *E* of the pile support and the *SRR*. In these tables, K_p is the Rankine's passive earth pressure coefficient,

σ_s is the pressure acting on the subsoil, σ_s' is the equivalent uniform stress on the subsoil, s is the centerline space between adjacent piles, s' is the clear spacing between adjacent piles, b is the width of the pile cap, W_{total} is the weight of the embankment fill, δ is the ratio of the width of the pile cap to the centerline space between adjacent piles, q is the uniform surcharge acting on the embankment fill, H is the embankment fill height, p_c is the vertical stress acting on the pile cap, s_x and s_y are the spacings in the x- and y-directions, respectively, $F_{GRsquare}$ is the total vertical load exerted by the 3D hemispheres on the square subsurface, $F_{Grstrips}$ is the total load on the GR strips, T is the total GR tensile force, t is the soft-ground deflection midway between the cap beams reinforced with the geotextile, D is the depth of the soft ground, γ_s is the unit weight of the embankment fill, E_a and E_m are the efficacy components corresponding to the arching and membrane effects, respectively, and K_G is the tensile stiffness of the geotextile. SSR^a is the SRR induced by the arching effect, SSR^m is the SRR induced by the membrane effect, p is the uniformly distributed surcharge on top of the fill (top load), and θ is the deflected angle of the geosynthetic.

Table 1. The calculation method of a pile-supported embankment without geosynthetic reinforcement.

Source	Load Supported by Pile A	Subsoil Load *C*	Efficacy *E* of the Pile	Stress Reduction Ratio (SRR)
Hewlett and Randolph [13]	$A = \frac{2K_P}{K_P+1} s^2 \sigma_s \left[(1-\delta)^{(1-K_P)} - (1-\delta)(1+K_P\delta)\right]$ where $\delta = b/s$	$C = W_{total} - A$	$E = \frac{\beta}{1+\beta}$, where $\beta = \frac{2K_P}{K_P+1} \frac{1}{1+\delta} \left[(1-\delta)^{-K_P} - (1+K_P\delta)\right]$	-
Low and Tang [21]	$A = K_P \sigma_s' s(1-\delta)\left[(1-\delta)^{-K_P} - 1\right]$	$C = W_{total} - A$	$E = \frac{\beta}{\beta+1}$ where $\beta = K_P\left[(1-\delta)^{-K_P} - 1\right]$	$SRR = \frac{\sigma_s'}{\gamma H}$
Abusharar et al. [46]	$A = W_{total} - C$	$C = (s-b)\sigma_s$, where $\sigma_S = \frac{\gamma_S(s-b)(K_P-1)}{2(K_P-2)} + \left(\frac{s-b}{s}\right)^{K_P-1} \left[q + \gamma_S H - \frac{\gamma_S s}{2}\left(1 + \frac{1}{K_P-2}\right)\right]$	$E = 1 - \left[\begin{array}{c} \frac{(s-b)^2(K_P-1)}{2sH(K_P-2)} + \left(\frac{s-b}{s}\right)^{K_P} \\ \left[1 + \frac{q}{\gamma_S H} - \frac{s}{2H}\left(1 + \frac{1}{K_P-2}\right)\right] \end{array}\right]$	-
BSI (2010) [23]	-	$C = 1.4\gamma(s-b)(s^2-b^2)X$, where $X = s^2 - b^2$ $(p_c'/(\gamma H + p))/(s^2-b^2)$	$E = 1 - \frac{(s^2-b^2)}{s^2}X$	-
Van Eekelen et al. [32,33,50]	$A = (\gamma H + p) \cdot S_x \cdot S_y - F_{GRsquare} - F_{GRstrips}$	$C = W_{total} - A$	$E = \frac{A}{W_{total}}$	-
Zhuang et al. [51]	$A = 2(s-b)\frac{K_P}{K_P+1}\left[s\left(1-\frac{b}{s}\right)^{-K_P} - s - K_P b\right]\sigma_S$	$C = W_{total} - A$	$E = \frac{A}{W_{total}}$	$SRR = \frac{\sigma_S}{\gamma H}$

Table 2. Calculation methods for a pile-supported embankment with geosynthetic reinforcement.

Source	Load Supported by Pile A + B	Subsoil Load C	Efficacy E of the Pile	Stress Reduction Ratio (SRR)
Low and Tang [21]	$A + B = W_{total} - C$	$C = \sigma_s' s' - 2K_G(\theta - \sin\theta)$	$E = (A+B)/(\gamma H A_i)$	$SRR = \frac{\sigma_s' s' - 2K_G(\theta - \sin\theta)}{s' \gamma H}$
Abusharar et al. [46]	$A + B = W_{total} - C$	$C = s'\left(\sigma_s - \frac{tE_c}{D}\right)$	$E = 1 - \frac{C}{s(\gamma_s H + q)}$	-
Pham [52–54]	$B = 8bT\sin\theta$	-	$E = E_a + E_m$, where $E_a = 1 - \left(1 - \frac{a^2}{s^2}\right) \cdot SSR^a$ $E_m = \frac{B}{(\gamma H + q)s^2}$	$SSR = \frac{\sigma_s}{\gamma H + q} = SSR^a - SSR^m$

2.3. The Characteristics of Stress and Settlement in Pile-Supported Embankments

Many researchers have studied the performance of foundations, which are monitored in terms of the settlement and vertical stress through field measurements, numerical simulations, and theoretical analyses. In this section, the characteristics of pile-supported embankments and the development pattern of soil arching under the effect of settlement and vertical stress are discussed.

2.3.1. Stress State

Several researchers have investigated the load distribution pattern on pile-supported embankments through experiments, field measurements, or numerical simulations. For example, Chen [55] set up a model test system and found that a taller embankment results in a higher stress concentration ratio, consistent with that reported by Han and Murugesan [56,57]. Nguyen [58] also found that the efficacy *E* increases with increasing embankment height.

The load distribution varies during the construction of the embankment and the consolidation of the subsoil. As shown in Figure 8 [59], the vertical stress on the subsoil increases linearly with the construction of the embankment. However, a decreasing tendency is observed after construction. Moreover, the excess pore water pressure gradually decreases to zero after construction, as shown in Figure 9 [60]. From this, it may be inferred that the consolidation of the foundation resulted in an excess decrease in the pore water pressure, leading to a decrease in the subsoil stress [61]. Moreover, the load distribution on the pile cap increases slightly during subsoil consolidation, as reported previously [62–64]. This might be explained as follows: the consolidation of the soil expends the differential settlement between the pile and subsoil, thus improving the soil-arching effect and enhancing the load transfer.

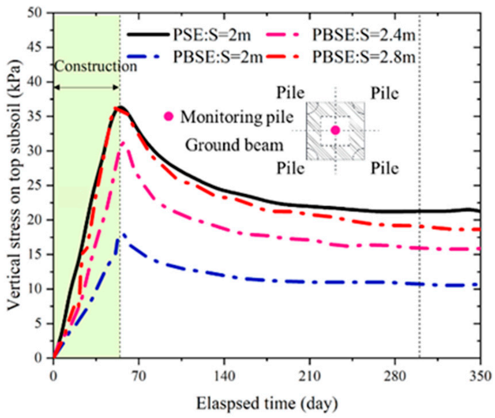

Figure 8. Vertical stresses on subsoil surface varying with time [59].

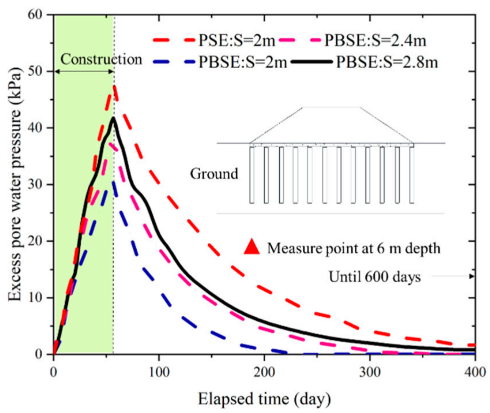

Figure 9. Variation of excess pore water pressures at the centerline of the embankment [59].

As shown in Figure 10 [65], the oblique dotted line is the overburden stress from the embankment and pavement, and the two horizontal dotted lines represent the outer and inner radius surfaces of the soil arching respectively. During soil consolidation, the vertical stress first increases, then decreases, and finally increases with increasing soil thickness (the distance from the bottom increases, as shown in Figure 10). The increase in the vertical stress is due to the increase in the soil thickness, and the decrease in the vertical stress is due to the soil-arching effect, which results in a stress transfer from the subsoil to the piles.

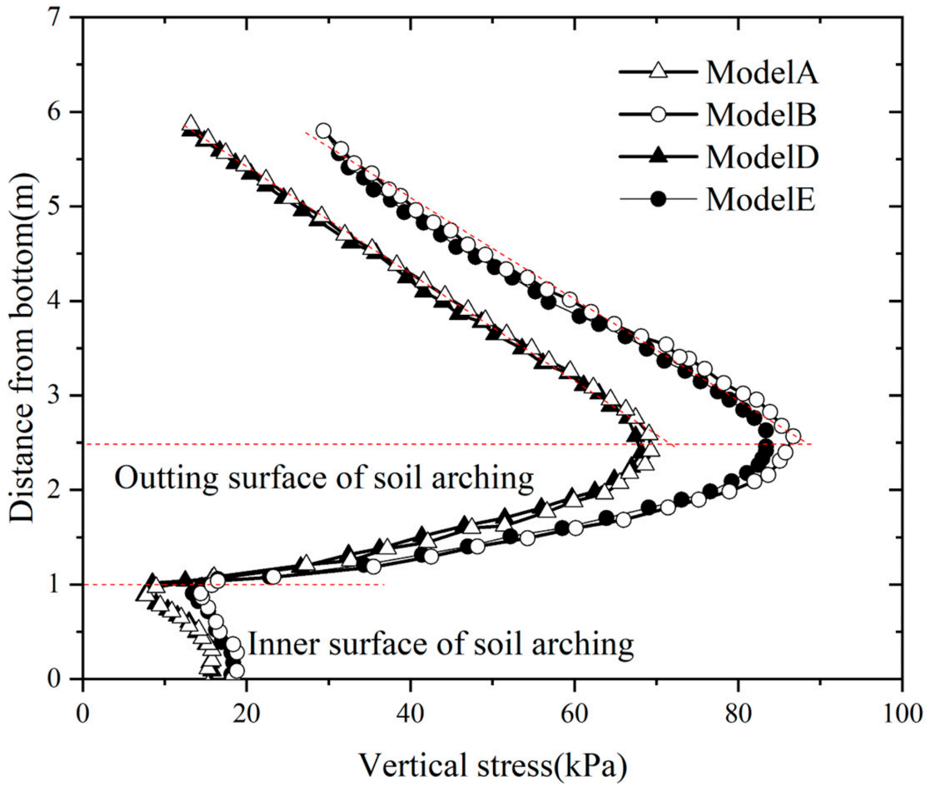

Figure 10. Distribution of vertical stress along the depth of embankment [65].

Recently, several researchers have focused on the vertical stress distribution on pile-supported embankments; however, few have studied the distribution of the horizontal stress or bending moment. For this case, Zheng and Ma [66,67] set up a separate numerical simulation model and found that the bending moment was at its maximum at the clay–sand interface and that it decreased sharply near the sand. However, the results were derived for the end-bearing pile embankment case, and the bending moment distribution in the floating pile embankment should be further investigated.

2.3.2. Settlement

Soil settlement behavior can be visualized by field monitoring or numerical simulation [60,68–71]. Evidently, the settlement increases during construction and continues to increase thereafter, though at a lower rate. This is because the excess pore water pressure dissipates during subsoil consolidation. There is differential settlement between the pile and subsoil, as reported by Hosseinpour [68,69] and Wang [60]. The differential settlement continues to expend during subsoil consolidation, almost accounting for half of the final differential settlement, as shown in Figure 11.

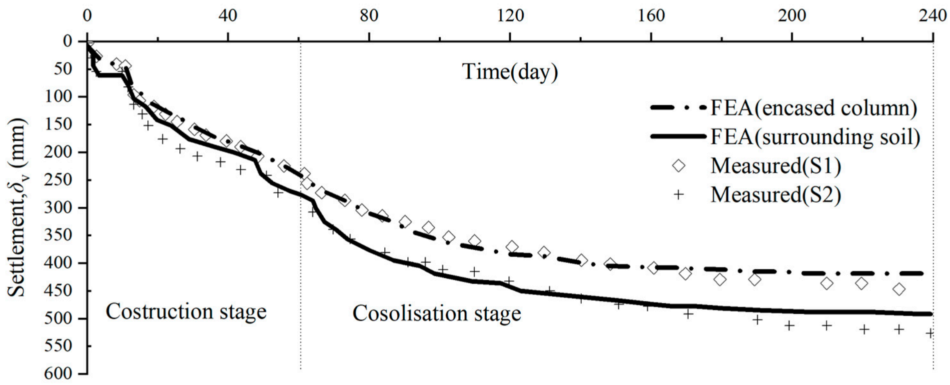

Figure 11. Computed (FEA) and measured settlements on encased column and surrounding soil.

However, the results differ from those reported by Zhang and Pan [70,71], who found that the differential settlement between the pile and subsoil was small, being even lower than 1%, as shown in Figure 12a,b. This result can be explained as follows: the former result is based on an end-bearing pile embankment whereas the latter is based on a floating pile embankment. Hence, it would be interesting to investigate the differences in the settlement behaviors between end-bearing and floating pile embankments.

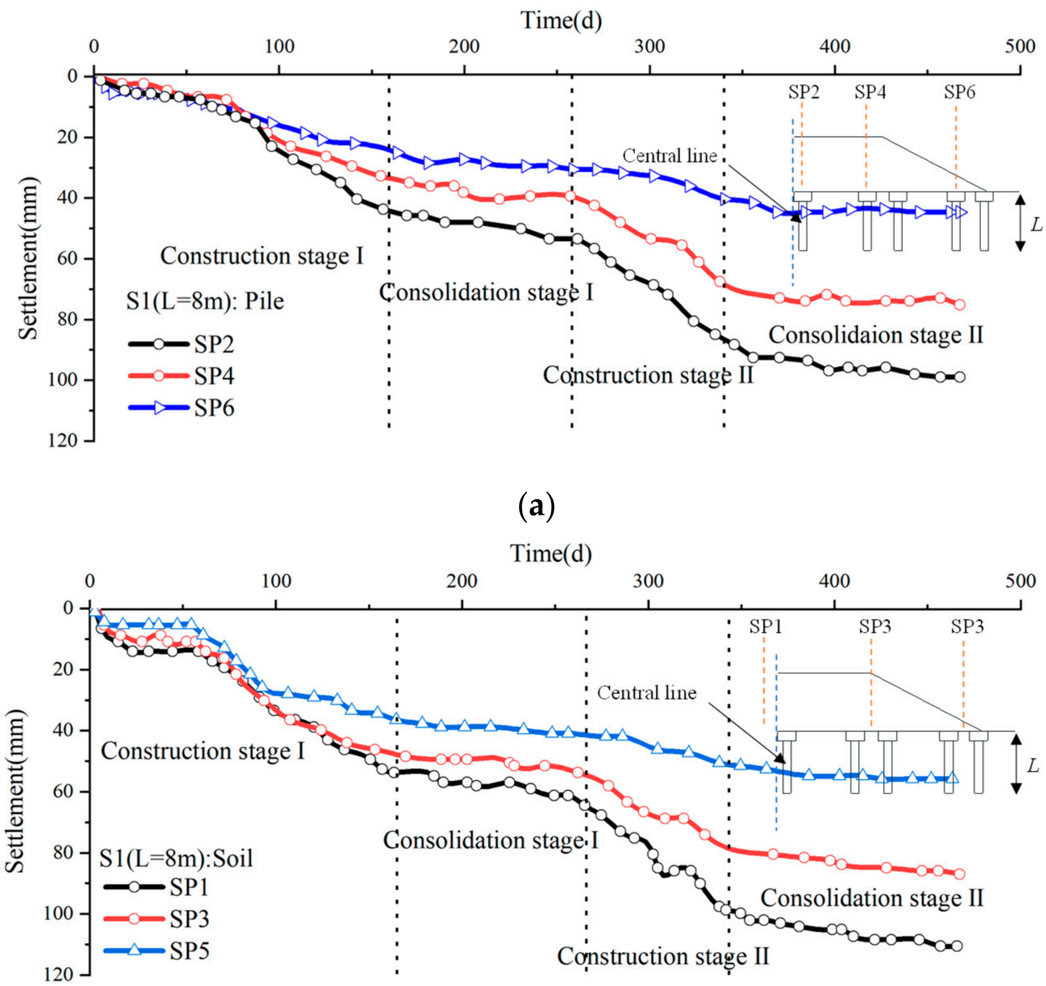

(**a**)

(**b**)

Figure 12. Temporal evolution of settlement at. (**a**) The piles of S1; (**b**) the soil of S1.

Based on the time evolution of pile and soil settlement, Pan [71] proposed the pile–soil settlement ratio (η) to evaluate the effect and evolution of soil arching, which is equal to the ratio of the settlement of piles and soil to the filling height. As shown in Figure 13, in the first filling stage, η firstly decreases with H value and then increases with H value. Finally, η tends to stabilize. This indicates that the soil arching was not formed and functioned until the filling height reached 1.4 ($s - b$). Then, the soil arching gradually formed and the pile settled faster than the soil. Finally, the soil arching was fully formed and the settlement ratio tended to a stabilized value.

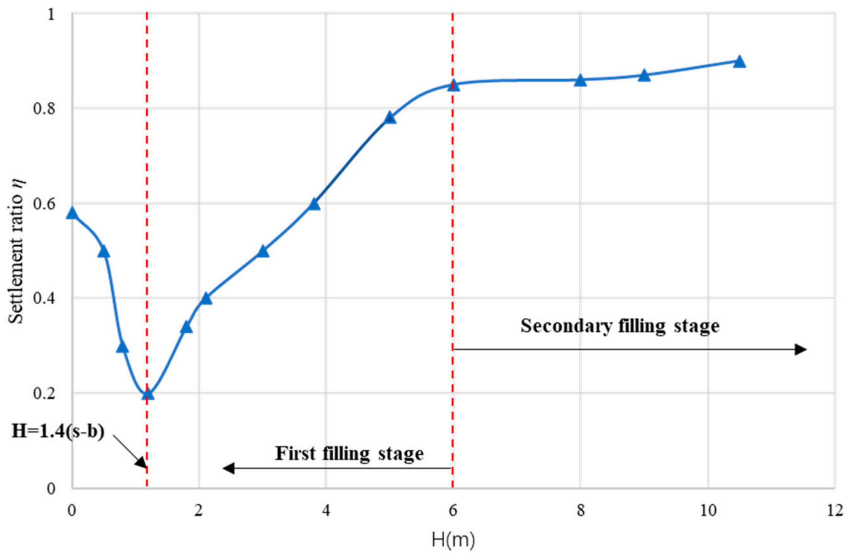

Figure 13. Evolution of settlement ratio of pile and soil with filling height.

As shown in Figure 14 [65], with the increase in the distance from the bottom, the settlement at the pile cap increases while the settlement on the subsoil decreases. From a certain height, the settlements at the pile cap and subsoil are equal. Therefore, this height is called the critical height, and the plate along which the settlement is equal is called the plane of equal settlement. The details of the critical height are introduced in the next section.

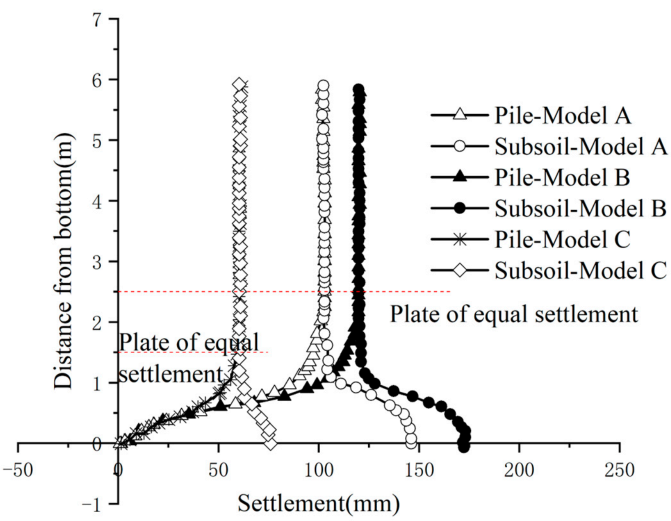

Figure 14. Distribution of settlement along the depth of embankment [65].

More recently, most researchers [65,72–74] have investigated the deformation behavior of pile-supported embankments under cyclic loading. Evidently, the settlement of a pile-supported embankment will increase with the number of cycles, velocity, and vehicle wheel load. Some researchers have also revealed that a geogrid can limit the deformation of a pile-supported embankment [75]. More studies should be conducted on the deformation behavior of pile-supported embankments under cyclic loading conditions, particularly considering the moisture content in the soil.

2.3.3. The Development of Soil Arching

Most current studies on soil arching in pile-supported embankments are based on a full and stable soil-arching model. In practice, the development pattern of soil arches includes many different stages and soil arching shapes.

Lai [76,77] divided the evolution of soil arching into three stages: development, forming–failure–re-forming, and dissipation. In the first stage, the soil arch forms gradually, and the load-sharing ratio of the piles increases. In the second stage, with increasing surcharge, the soil arching undergoes a development phase, a steady phase, destruction, and re-formation. In the final stage, the embankment cannot form a new stable soil arch once the surcharge exceeds a certain value. Interestingly, Stage 3 does not occur in a pile-supported embankment with a geogrid reinforcement during the entire construction [76].

And, Lai [77–79] also divided the soil arch into three shapes: shear plane arching [80,81], partial arching [82], and full arching [83]. As shown in Figure 15, the three types of arching are associated with an inactive region ($d_{\mathrm{ef}} < 1/16\Delta s$: located above the piles), an active region ($d_{\mathrm{ef}} > 15/16\Delta s$: a sliding region that is located above the trap-wall), and a transition region ($1/16\Delta s < d_{\mathrm{ef}} < 15/16\Delta s$: between the inactive and active regions). And, d_{ef} is the displacements of embankment fill, and Δs is the pile–subsoil relative displacement. However, compared with shear plane arching and partial arching, there is an equal settlement region in the full arching case. Evidently, there is no differential settlement in the equal settlement region. Thus, the height of the bottom of the equal settlement region is defined as the critical height.

Rui [34,84,85] also divided the shapes of the soil arch into three types: triangular arching (a triangular deformation region occurs in the model), tower-shaped arching (a tower-shaped deformation region occurs in the model), and equal settlement arching (an equal settlement region occurs in the model). A solution is proposed based on the equal settlement arching.

Based on the theoretical analysis experiment, numerical simulation, and field monitoring, several researchers have established calculation methods for the critical height. The calculation equations differ depending on the investigation method employed (theoretical analysis, experiments, numerical simulation, or field monitoring), the calculation model used, and the embankment type selected. Table 3 presents these equations in detail. In this table, s is the center space between adjacent piles, b is the width of the pile cap, and H is the total height of the embankment fill.

Table 3. Calculation method of critical height.

References	Critical Height	
Terzaghi [12]	$2.0(s-b)$	Pile-supported embankment without geogrid reinforcement
Han and Gabr [56]	$1.3(s-b)$	-
Handy [27]	$(0.4 \sim 0.45)H$	In the case of full soil arching
Van Eekelen [32]	$(0.51 \sim 0.62)(s-b)$	Numerical studies and field measurements of geosynthetic-reinforced pile-supported embankments
Xu [86]	$(1.1\sim 1.5)(s-b)$	A geosynthetic-reinforced pile-supported (GRPS) embankment
Chen [87]	$1.4(s-b)$	Laboratory model
Rui [34]	$1.75(s-b)$	-
Lee [88]	$(2.0\sim 3.25)(s-b)$	-
Lai [78]	$0.8(s-b)$	Un-reinforced pile-supported embankments
BSI (2010) [23]	$1.4(s-b)$	-
Samira [89]	$1.18(s-b)$	-
Chen [90]	$(1.0 \sim 1.5)(s-b)$	-

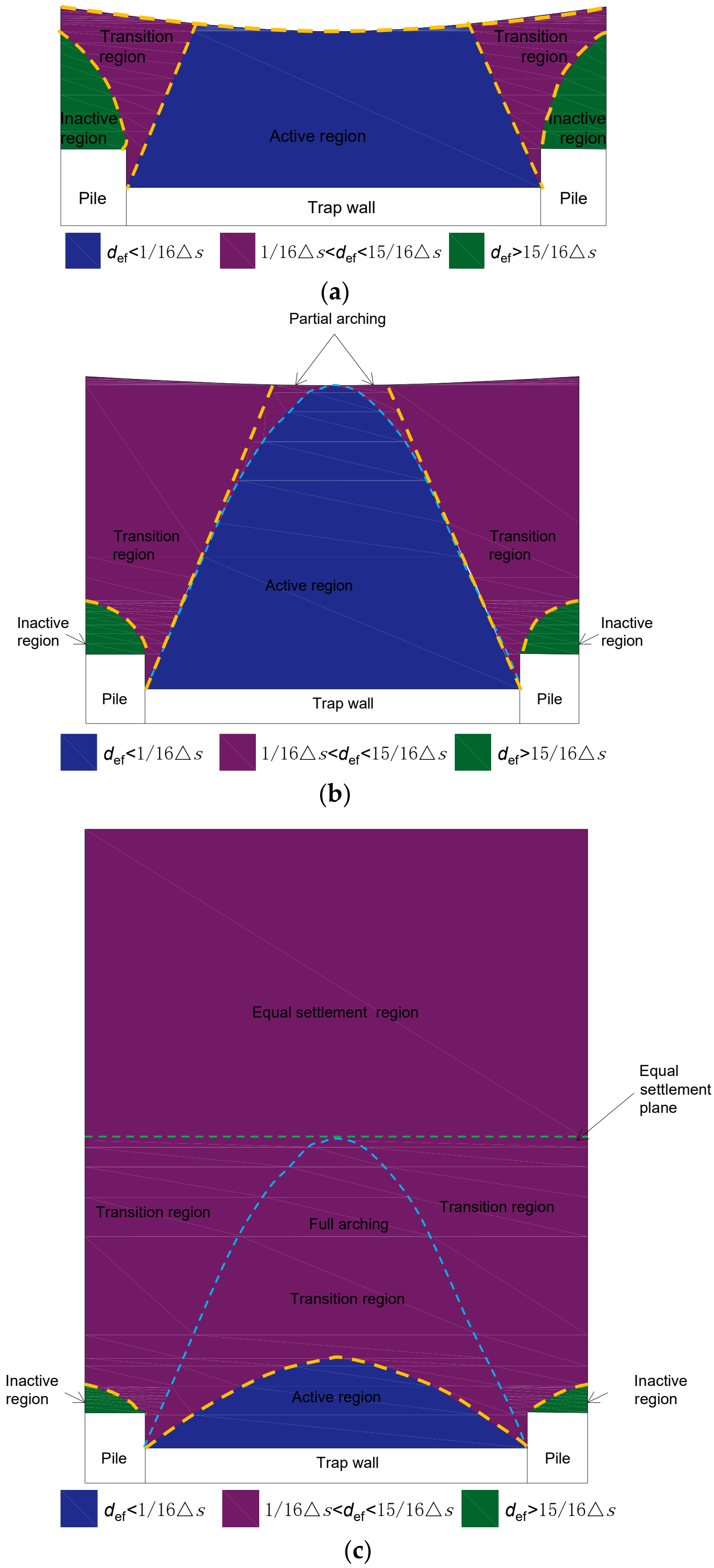

Figure 15. Different types of soil arching. (**a**) Without soil arching. (**b**) Partial soil arching. (**c**) Full soil arching.

3. Factors Influencing Soil Arching

The Soil-arching effect, which is a typical phenomenon in soil mechanics, is widely used to introduce the load distribution and soil deformation in pile-supported embankments. To better understand the mechanism of the soil-arching effect in pile-supported embankments, it is necessary to explore the factors influencing the soil-arching phenomenon. A pile-supported embankment comprises an embankment fill, piles, and subsoil. The effect of the geogrid reinforcement should be considered in GRPS embankments. Therefore, in this section, the following factors influencing the soil arching phenomenon are discussed: piles, embankment fill, subsoil, and geogrid.

3.1. Piles

In the past twenty years, researchers have widely studied the influence of piles on soil arching using various methods, including laboratory investigations [86,91,92], field data and analytical solutions [90,93], 2D discrete element method models [92,94], 2D finite element models [95,96], and 3D finite element models [95,97–99]. The main conclusions drawn in the aforementioned studies are summarized below.

3.1.1. Pile Shape

- $H/(s-a)$ directly influences the soil-arching effect in a pile-supported embankment. A higher $H/(s-a)$ generally leads to a higher maximum E, which represents a higher soil-arching effect. A lower $H/(s-a)$ will result in a higher settlement due to the lower degree of soil arching.
- Different values of the coefficient $H/(s-a)$ for pile-supported embankments result in different types of soil arching shapes (discussed in Section 2.3.3). Thus, the minimum height of the embankment fill, under which a full soil arching can be formed, should be considered in the design, in order to give full play to the soil-arching effect to enhance the load transfer.
- With the increase in the spacing between adjoint piles, the soil-arching effect decreases. However, for a given final embankment height, within the scope of the pile spacing, the net cap spacing can be increased without significantly affecting the pile efficiency.
- The soil-arching effect increases with the increase in the pile cap size (this is also observed with the decrease in the clearance spacing between the pile caps).
- For a given pile spacing and embankment height, the longer the pile length, the higher the maximum pile efficiency and replacement ratio and the higher the efficiency, indicating a greater soil-arching effect.
- The shape of the pile body has the most significant influence on the soil-arching effect in the case of the floating-pile embankment. For instance, the load sharing ratios from the sections improved by tube piles are significantly lower than those from the sections improved by Y-shaped piles.

3.1.2. Pile Arrangement

- In a triangular arrangement of the pile-supported embankment, there are two types of soil arching: primary soil arching (between the upper and lower boundaries) and secondary soil arching (below the lower boundary). The primary soil arching mainly plays the role of transferring the load onto the pile caps, and the secondary soil arching transfers the load toward the area between the pile caps. The height to the crown of the arch above the triangular arrangement is lower than that in the case of the square arrangement.
- Compared with the square arrangement of a pile-supported embankment, the triangular arrangement of the piles has a greater soil-arching effect, owing to which a higher embankment load is transferred to the piles, resulting in a lower settlement at the top of the subsoil.

3.1.3. Pile Types

- Regardless of the type of embankment (end-bearing pile embankment or floating pile embankment), the variation in the load distribution with time or embankment height is similar, though there are some differences. The details of the load distribution have been discussed in Section 2.3.1.
- Compared with the end-bearing pile embankment, the floating pile embankment after construction exhibits a greater settlement, as shown in Section 2.3.2. The consolidation settlement accounts for 50–60% of the total settlement in the floating pile embankment, whereas it is small enough to be ignored in the case of the end-bearing pile embankment.
- End-bearing piles carry more load than floating piles, owing to the soil arching and tensioned membrane effects, leading to a greater settlement in the floating pile embankment.

3.2. Embankment Filling

The embankment filling, which is one of the important components in a pile-supported embankment, influences the soil arching and load distribution on the pile-supported embankment, significantly changing the settlement of the pile-supported embankment. Most current researchers [100–102] focused on the influence of the embankment height, which is mentioned in Section 2.3.2. However, studies on the materials used in the embankment filling are limited. Some studies have shown that the parameters related to the embankment filling (such as the cohesion and friction angle) influence the soil-arching and membranate effects, and the impact is more pronounced in the case of the GRPS embankment.

Xu [86] investigated the influence of the cohesion of the embankment fill on the pile-supported embankment and found that the fill cohesion can enhance the soil-arching effect and transfer more load to the pile caps, which reduces the load transfer to the geosynthetic reinforcement and the subsoil, resulting in a small settlement and a lower critical height. Bhasi [103] proposed more details regarding the influence of fill cohesion on pile-supported embankments. With the increase in the cohesion from 0 to 10 kPa, the ratio of the load carried by the piles to the total embankment load increases, and the settlement is reduced. However, for cohesion beyond 10 kPa, the result does not change. The cohesion is not widely used due to its long-term unreliability, as mentioned previously [7].

In addition to the cohesion, the fill friction angle significantly influences the soil-arching effect. With increasing friction angle, the soil arching is enhanced, the membrane effect is reduced, and the total efficacy of the soil arching and membrane effects is improved [52,101,103,104], resulting in a lower total settlement. With increasing friction angle, the differential settlement between the pile and subsoil increases, which may enhance the soil-arching effect, as reported by Meena [96].

In the different ranges of the friction angle, the effect of the friction angle on soil arching is different. Bhasi [103] found that a higher friction angle can enhance the magnitude of the load transferred to the piles within a friction angle of 30°, which is reported by Jenck [105]. However, Wijerathna [99] found that the sensitivity of the friction angle on the ratio of the load carried by the piles to the total embankment load increases with an increase in the friction angle from 32° to 38°. The different results might be attributed to the difference in the types of embankments and the method of investigation. The former investigated the effects of the friction angle in the end-bearing pile-supported embankment, while the latter did so in the floating pile-supported embankment. Hence, more studies on the influence of the fill friction angle on the embankment should be conducted

3.3. Subsoil

Several researchers [100,106–108] have investigated the influence of subsoil on pile-supported embankments in terms of the modulus ratio between the pile and the subsoil, cohesion, friction angle, compression index (C_c), and over-consolidation ratio. The aforementioned factors have different influences on the embankment under different conditions:

end-bearing or floating piles, with or without geosynthetic reinforcement, and water levels in the subsoil. Some of the conclusions drawn in the above studies are as follows:

- Soil strength parameters (cohesion, friction angle, and Young's modulus) can improve the arching effects but cannot change the shape or prohibit the development of the arching zone for soils whose displacements are sufficient for initial plastic flow.
- A higher modulus ratio between the pile and subsoil will increase the difference in the differential settlement between the pile and subsoil, thus improving the soil arching and increasing the stress ratio. However, if the modulus ratio is greater than 50, the increase rate will be low.
- With the increase in the compression index (C_c), the development of subsoil settlement is accelerated, which accelerates the evolution of the soil arching and increases the stress borne by the geogrid.
- A higher OCR can significantly suppress the growth of subsoil settlement, which decreases the contribution of the geogrid in carrying the embankment load.
- For the GRPS embankment, the compressibility of the underlying soil does not influence the load transfer mechanism. However, there is a complementary action between the underlying soil and the geosynthetic sheet. A higher compressibility of the underlying soil can limit the movement of the embankment soil, which decreases the displacement of the geosynthetic sheet.

3.4. Geosynthetic Reinforcement

3.4.1. The Properties of Geosynthetic Reinforcement

A geosynthetic reinforcement is widely employed in pile-supported embank ments [109,110]; the tension provided by the reinforcement provides support and limits the lateral spreading of the embankment, and a higher embankment load is transferred to the pile cap. Engineering practice indicates that during construction, a geogrid can absorb the stress until an arch is formed, which limits the lateral movement of the soil and improves the safety of construction.

The geogrid stiffness, which is one of the main factors of the maximum geogrid tension, has also been widely investigated [52,56,111]. Han [56] and Zhuang [111] proposed that the maximum tension in a geogrid increases with increasing stiffness. Zhuang's results also point out that the aforementioned law applies to both static and dynamic conditions, although the tension might be slightly greater for the same geogrid stiffness under the dynamic load. Pham [52] also obtained a similar result; the results of linear and nonlinear subsoil models deviated more with an increase in the stiffness of the geosynthetic. The author also proposed that the membrane action of the geogrid is strengthened as the geogrid becomes stiffer, resulting in a lower deflection.

Recently, most investigations on GRPS embankment reinforcements have been based on the isotropic membrane [56,68,100,112]; a geogrid is an orthotropic material, with nonzero stiffness only in two orthogonal directions. Therefore, the numerical simulation of a GRPS embankment, whose geogrid is simulated using an isotropic membrane, cannot completely match the field conditions.

Zhuang [113] found that the maximum geogrid tension increases with the geogrid stiffness. This indicates that the influence of the geogrid stiffness on the maximum geogrid tension decreases with increasing stiffness. The results of the orthotropic membrane model match those of the truss element model, whereas the results of the isotropic membrane model tend to produce values that are 22–58% greater. This indicates significant differences between the orthotropic and isotropic membrane models. Hence, different geogrid materials should be considered for GRPS embankments.

By conducting a series of plane-strain (2D) trapdoor tests, Al-Naddaf [42] also showed that a geogrid can maintain a more stable arch and lower the height of the equal settlement plane. They also found that a biaxial geogrid was more effective in carrying the load than an uniaxial geogrid with similar tensile strength and stiffness, owing to its better lateral restraint.

3.4.2. The Number of Geogrid Layers

Several researchers [98,114–116] have investigated the influence of the number of geogrid layers on GRPS embankment. By conducting three centrifuge model tests, Shen [115] found that changing the number of geogrid layers from two to one did not significantly change the settlement of the foundation soil, and the influence on the load distribution was also not noticeable. Xu [114] reported a similar phenomenon: for Models T1-T4 (the T1 without a geogrid layer while the T2, T3, and T4, respectively, with one, two, and four geogrid layers), the embankment settlement decreased significantly with the addition of reinforcement layers, but the differences in the settlement for embankments with one, two, and four geogrids were small. This indicates that the influence of the number of geogrid layers on the embankment settlement is small.

Figure 16 [98] shows the relationship between the differential settlement efficacy and geogrid with different numbers of layers and vertical spacing between the layers. Evidently, the differential settlement increases with the increase in the number of geogrids or with the decrease in the vertical spacing between the geogrid layers. Badakhshan [116] also found that the differential settlement decreases with the increase in the number of geogrids. Moreover, two layers of geogrids placed optimally can more effectively decrease the differential settlement than using one stiffer geosynthetic layer. This indicates that the differential settlement has a greater dependency on the number of geogrid layers than the stiffness of the geogrid.

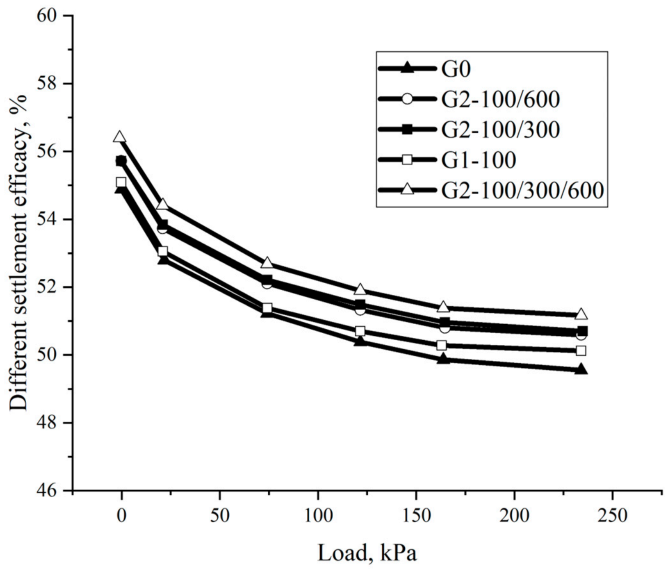

Figure 16. Variation in differential settlement of efficacy with the surcharge load [98].

3.4.3. Strain in the Geogrid

The strain is an important parameter of a pile-supported embankment and is influenced by many factors, making it difficult to measure. During the construction, the strain increases with increasing fill height. The strain decreases in the short-term after construction due to the redistribution of the stress on the embankment fill under the effect of pile settlement. Thereafter, the strain in the geogrid increases until it reaches a constant value. During and after preloading, the strain first increases and then decreases, and the maximum tensile deformation during preloading was found to be 2.92 times that at the end of surcharge filling, as reported by Cao [117]. This indicates that the creep of the geogrid should be considered to ensure safety during long-term serviceability. Al-Naddaf [42] found that regardless of the number of geogrid layers used (single or double) in the embankment, the maximum tensile strain occurred at the trapdoor edges. At the trapdoor centerline, the upper geogrid layer exhibited a significantly lower strain than the lower geogrid layer.

Figure 17 [118] shows the geogrid strain at different locations with the increase in the number of load cycles. Evidently, the geogrid strain increases with the number of load cycles, and the increased rate increases with an increase in the load cycles. Notably, the strain at sg3 decreases within five cycles because the soil particles above the geogrid move or slide toward the centerline, generating an inward shear stress that compresses the geogrid.

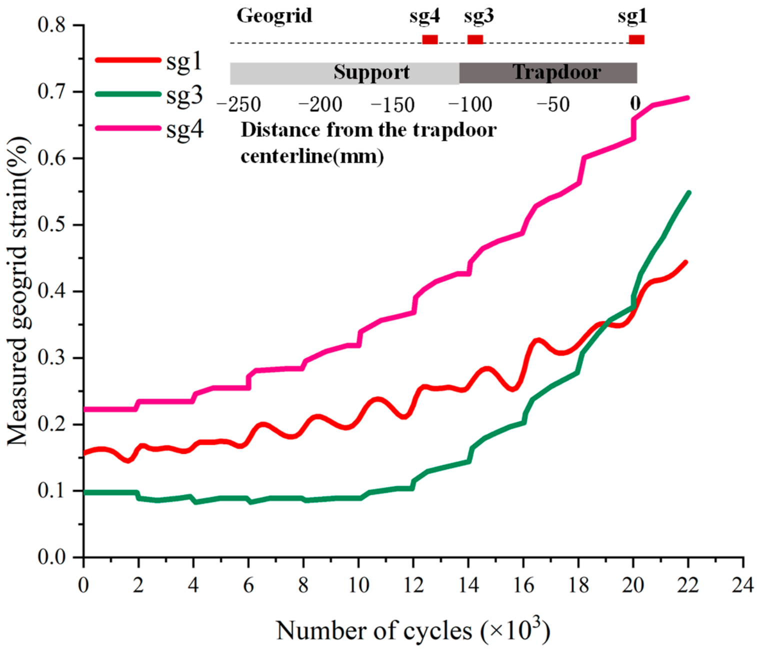

Figure 17. Progressive development of strains at sg1, sg3, and sg4 [118].

Shen [119] reported differences in the geogrid strain between end-bearing and floating pile embankments. The geogrid strain in the end-bearing pile embankment was lower than that in the floating pile embankment. The geogrid strain was at its maximum at the center of the end-bearing pile embankment, whereas the maximum strain of the model geogrid occurred near the shoulder of the floating pile embankment.

4. Concluding Remarks

This section provides a summary of the principal conclusions from this paper.

4.1. Load Distribution in Soil

Soil arching is a mechanical phenomenon in which pressure is transferred from the part with a lower stiffness or greater movement to the part with a higher stiffness or lower movement. Several researchers have attributed this phenomenon to shearing resistance, which causes the pressure transfer between the aforementioned parts.

Current studies on soil arching or load distribution are based on trapdoor models, 2D equal-thickness semicircle soil arch models, 3D equal-thickness shell soil arch models, and models extended from these. The load on an embankment can be divided into two parts: the load supported by piles (referring to A + B) and the load supported by the subsoil between the piles (referring to C). For the GRPS embankment, the load supported by the piles can be further divided into part A (soil-arching effect) and part B (membrane effect). The load distribution and soil-arching development are represented by E and SSR, respectively.

The results obtained by theoretical methods, experiments, field monitoring, and numerical simulations have shown that the vertical stress increases during construction and then decreases during soil consolidation due to the dissipation of the excess pore water pressure.

4.2. Deformation in Soil

During embankment construction, the soil arching undergoes three stages: development, forming–failure–reforming, and dissipation. Influenced by the development of the soil arch, the differential settlement between the pile and subsoil increases gradually until the values tend to stabilize. And, during the consolidation, the differential settlement increases slightly due to the load redistribution, leading to the re-formation of the soil arch.

Influenced by the total height of the embankment, there are three types of soil arching: shear plane arching, partial arching, and full arching. The types of soil arching are related to the value of $H/(s-a)$. For an embankment with full arching, there is an equal region wherein the soil settlement at the same height is equal. The height of the bottom of the equal-settlement region is defined as the critical height, which is related to the pile spacing. Below the critical height, the differential settlement decreases gradually with increasing height due to soil arching.

4.3. Factors Influencing Soil Arching

Soil arching influences the load distribution and settlement and is affected by the following factors: piles, embankment filling, subsoil, geogrid, and environment. These factors can be explained as follows:

- Piles with a larger width, smaller spacing, and higher length can improve the soil arching on the embankment, which enhances the load transfer from the subsoil to piles and decreases the settlement.
- Compared with the square arrangement of the pile-supported embankment, the triangular arrangement of piles brings about a greater soil-arching effect, which increases the embankment load transferred to the piles, resulting in a smaller settlement at the top of the subsoil.
- The settlement on a floating pile embankment after construction is greater than that on an end-bearing pile embankment. The consolidation settlement accounts for 50–60% of the total settlement in the floating pile embankments, whereas it is small enough to be ignored on end-bearing pile embankments.
- The shape of the pile body and the pile length have a greater influence on the floating pile embankment. This is mainly because the bearing capacity of a floating pile depends on the side friction resistance, whereas that of the end-bearing pile depends on the pile diameter and strength of the layer-bearing soil.
- An embankment fill with a higher cohesion and friction angle can improve the soil-arching effect, which enhances the load transfer between the subsoil and piles. However, the aforementioned rule is only applicable in a specific range of the cohesion and friction angle.
- The soil strength parameters (cohesion, friction angle, and Young's modulus) can improve the soil-arching effect but cannot change the shape or prohibit the development of the arching zone in soil whose displacements are sufficient for initial plastic flow.
- A higher compression index will accelerate the development of subsoil settlement and accelerate the evolution of the soil arch.
- There is a complementary action between the underlying soil and the geosynthetic sheet. The higher compressibility of the underlying soil limits the movement of the embankment soil, which decreases the displacement of the geosynthetic sheet.
- The geogrid in the embankment can provide support and limit the lateral spreading of the embankment, and a higher embankment load is transferred to the pile cap. With increasing stiffness, a geogrid will exhibit a higher tension, which applies to embankments under static and dynamic conditions.
- Orthotropic and isotropic membrane models produced results with some differences, indicating that different materials of the geogrid should be considered for GRPS embankments.
- There were differences in the load distribution and soil settlement for embankments with or without the geogrid. However, the influence of the number of geogrid layers

for embankment settlement was small. The number of geogrid layers and the spacing between geogrids had the most significant influence on the differential settlement.

- For the GRPS embankment, the maximum tensile deformation occurred at the edge of the pile cap. During long-term serviceability, the geogrid will strain continually, indicating that the creep of the geogrid should be considered.

5. Future Prospects

The soil arching, load distribution, deformation, and other factors influencing CPS and GRPS embankments have been investigated in current studies. These studies were based on end-bearing pile embankments under static conditions. Investigations in floating pile embankments are relatively fewer than that of the end-bearing pile embankments. In the past ten years, studies have also been conducted on embankments under cyclic loading. However, the conditions considered are relatively simple, yielding results that significantly deviate from the actual complex situation. Directions for future research are provided below:

- A comparison between end-bearing and floating pile embankments during construction, consolidation, and long-term operation can be made in terms of the load distribution.
- A comparison between end-bearing and floating pile embankments during consolidation can be made in terms of the total and differential settlements.
- The impact of changes in the water level in the embankment fill on soil arching can be studied.
- The impact of changes in the water level in the subsoil on the side friction of floating piles can be studied.
- The load distribution and soil deformation of the embankment under the combined effect of traffic load and water should be investigated.
- The distribution of the side-friction resistance of floating piles with the pile length, particularly the friction resistance at the interface between different types of soil layers, can be analyzed.
- Variations in the tension and strain of the geogrid during long-term operation can be explored.
- A suitable stiffness range for the geogrid should be determined; if the stiffness of the reinforced body is too low, it will have little effect on the soil-arching phenomenon; if the reinforcement has a large stiffness, it will have a lower ductility, and excessive deformation can lead to failure.

Author Contributions: Conceptualization, writing—review and editing, funding acquisition, K.W.; methodology, formal analysis, writing—original draft preparation, J.Y.; data curation, supervision, X.W.; validation, visualization, Z.Q. All authors have read and agreed to the published version of the manuscript.

Funding: This research was supported by the National Natural Science Foundation of China (Grant No. 52378467, No. 52109139 and No. 52278373).

Data Availability Statement: Not applicable.

Acknowledgments: This project was supported by Engineering Research Center of Ministry of Education for Renewable Energy Infrastructure Construction Technology. The authors would also like to thank all the reviewers who participated in the review.

Conflicts of Interest: The authors declare no conflicts of interest.

Notations

The following symbols are used in this paper:

A	total load is transferred to the pile through soil arching
B	load transferred to the piles through the reinforcement
C	load is borne by the subsoil
E	proportion of embankment weight carried by the piles
E_{a}	efficacy components corresponding to the arching effects
E_{m}	efficacy components corresponding to membrane effects
SRR	stress reduction ratio
SSR^{a}	SRR induced by the arching effect
SSR^{m}	SRR induced by the membrane effect
F_{GRsquare}	total vertical load exerted by the 3D hemispheres on the square subsurface
F_{GRstrips}	total load on the GR strips
W_{total}	weight of the embankment fill
H	embankment fill height
K_{p}	Rankine's passive earth pressure coefficient
K_{G}	tensile stiffness of the geotextile
L	width of the sliding plates
D	depth of the soft ground
p	uniformly distributed surcharge on top of the fill (top load)
b	width of the pile cap
c	cohesion of the soil
δ	ratio of the width of the pile cap to the centerline space between adjacent piles
q	uniform surcharge acting on the embankment fill
θ	deflected angle of geosynthetic
s	centerline space between adjacent piles
s'	clear spacing between adjacent piles
s_{x}	spacings in the x-directions
s_{y}	spacings in the y-directions
γ	unit weight of the soil
γ_{s}	unit weight of the embankment fill
T	total GR tensile force
t	soft-ground deflection midway between the cap beams reinforced with the geotextile
p_{c}	vertical stress acting on the pile cap
σ_{s}	pressure acting on the subsoil
${\sigma_{\mathrm{s}}}'$	equivalent uniform stress on the subsoil
σ_{k}	horizontal stress acting on the soil
σ_{v}	vertical stress at any depth into the soil
dz	thickness of a unit
z	depth of unit in Figure 4
d_{ef}	displacements of embankment fill in Figure 15
Δs	pile–subsoil relative displacement. However, this is compared with the shear plane in Figure 15.

References

1. Liu, H.L.; Li, H.; Peng, J.; Gao, Y.F. Indoor Experimental Study on Vacuum Heap Load Combined Preloading for Strengthening Soft Foundation. *J. Geotech. Eng.* **2004**, *26*, 145–149.
2. Xue, R.; Hu, R.L.; Mao, L.T. Fractal Study on Microstructure Changes during Soft Soil Reinforcement Process. *China Civ. Eng. J.* **2006**, *39*, 87–91. [CrossRef]
3. Zheng, Y.R.; Li, X.Z.; Feng, Y.X.; Zhou, L.Z.; Lu, X.; He, H.Y. Research on the Mechanism and Technology of Dynamic Compaction of Soft Clay Foundation. *J. Rock Mech. Eng.* **1998**, *17*, 571–580.
4. Liu, H.L.; Fei, K.; Ma, X.H.; Gao, Y.F. Vibration Sinking Mold Large Diameter Cast-in-Place Thin-Walled Pipe Piles Application (I): Development and Design. *Rock Soil Mech.* **2003**, *24*, 164–168. [CrossRef]
5. Bhasi, A.; Rajagopal, K. Numerical Study of Basal Reinforced Embankments Supported on Floating/End Bearing Piles Considering Pile–Soil Interaction. *Geotext. Geomembr.* **2015**, *43*, 524–536. [CrossRef]
6. Girout, R.; Blanc, M.; Thorel, L.; Dias, D. Geosynthetic Reinforcement of Pile-Supported Embankments. *Geosynth. Int.* **2018**, *25*, 37–49. [CrossRef]

7. Van Eekelen, S.J.M.; Han, J. Geosynthetic-Reinforced Pile-Supported Embankments: State of the Art. *Geosynth. Int.* **2020**, *27*, 112–141. [CrossRef]
8. Lewis, W.A. The Settlement of the Approach Embankments to a New Road Bridge at Lackford, West Suffolk. *Geotechnique* **1956**, *6*, 106–114. [CrossRef]
9. Rowe, R.K.; MacLean, M.D.; Barsvary, A.K. The Observed Behaviour of a Geotextile-Reinforced Embankment Constructed on Peat. *Can. Geotech. J.* **1984**, *21*, 289–304. [CrossRef]
10. Rowe, R.K.; Maclean, M.D.; Soderman, K.L. Analysis of a Geotextile-Reinforced Embankment Constructed on Peat. *Can. Geotech. J.* **1984**, *3*, 563–576. [CrossRef]
11. Terzaghi, K. Stress Distribution in Dry and in Saturated Sand above a Yielding Trap-Door. In Proceedings of the International Conference of Soil Mechanics, Harvard University, Cambridge, MA, USA, 22–26 June 1936; pp. 307–311.
12. Terzaghi, K. *Theoretical Soil Mechanics*; John Wiley and Sons: New York, NY, USA, 1943; pp. 307–311.
13. Hewlett, W.J.; Randolph, M.F. Analysis of Piled Embankments. *Ground Eng.* **1988**, *21*, 12–18.
14. Reid, W.M.; Buchanan, N.W. BRIDGE APPROACH SUPPORT PILING. In Proceedings of the International Conference on Advances in Piling and Ground Treatment, London, UK, 2–4 March 1983; ICE Publishing: London, UK, 1983; pp. 267–274.
15. Kempfert, H.G.; Stadel, M.; Zaeske, D. Berechnung von Geokunstst off bewerten Trags Chichten Über Pfahlelementen. *Bautechnik* **1997**, *74*, 818–825.
16. Kempfert, H.G.; Zaeske, D. Interactions in Reinforced Bearing Layers over Partial Supported Underground. In Proceedings of the Twelfth European Conference on Soil Mechanics and Geotechnical Engineering (Proceedings), Amsterdam, The Netherlands, 7–10 June 1999.
17. Carlson, B.O. *Armerad Jord Beräkningsprinciper För Banker På Pålar*; Terranova, Distr. SGI: Linköping, Sweden, 1987.
18. Guido, V.A.; Knueppel, J.D.; Sweeny, M.A. Plate Loading Tests on Geogrid-Reinforced Earth Slabs. *Proc. Geosynth.* **1987**, *87*, 216–225.
19. Jones, C.J.F.P.; Lawson, C.R.; Ayres, D.J. *Geotextile Reinforced Piled Embankments*; Balkema: Rotterdam, The Netherlands, 1990; pp. 155–160.
20. Kempton, G.T.; Jones, C.J.F.P. *The Use of High Strength Link Geotextiles over Piles and Voids*; Balkema: Rotterdam, The Netherlands, 1992; pp. 613–618.
21. Low, B.K.; Tang, S.K. Arching in Piled Embankments. *J. Geotech. Eng.* **1994**, *120*, 1917–1938. [CrossRef]
22. *BSI (1995) BS8006*; Code of Practice for Strengthened/Reinforced Soils and Other Fills. British Standards Institution: London, UK, 1995.
23. *BSI (2010) BS8006-1*; Code of Practice for Strengthened/Reinforced Soils and Other Fills. British Standards Institution: London, UK, 2010.
24. EBGEO. *Empfehlungen Für Den Entwurf Und Die Berechnung von Erdkörpern Mit Bewehrungen Aus Geokunststoffen—EBGEO*; Ernst & Sohn: Berlin, Germany, 2010.
25. Van Eekelen, S.J.M.; Brugman, M.H.A. *Design Guideline Basal Reinforced Piled Embankments*; CUR226; SBRCURnet: Delft, The Netherland, 2016.
26. Schaefer, V.R.; Berg, R.R.; Collin, J.G.; Christopher, B.R.; DiMaggio, J.A.; Filz, G.M.; Bruce, D.A.; Ayala, D. *Ground Improvement Methods—Reference Manual Vols. I and II*; FHWA-NHI-16-027 and FHWA-NHI-16-028 2017; Federal Highway Administration, U.S. Department of Transportation: Washington, DC, USA, 2017.
27. Handy, R.L. The Arch in Soil Arching. *J. Geotech. Eng.* **1985**, *111*, 302–318. [CrossRef]
28. Kellogg, C.G. Discussion of "The Arch in Soil Arching" by Richard L. Handy (March, 1985, Vol. 111, No. 3). *J. Geotech. Eng.* **1987**, *113*, 302–318. [CrossRef]
29. Railway Technology Research Institute. *The Design and Construction Handbook of Mixing Piled Foundation (Machine Mixing)*; Railway Technology Research Institute: Tokyo, Japan, 2001.
30. Nordic Geosynthetic Group. *Nordic Guidelines for Reinforced Soils and Fills*; Nordic Geotechnical Group: Stockholm, Sweden, 2004.
31. Kempfert, H.G.; Göbel, C.; Alexiew, D.; Heitz, C. German Recommendations for Reinforced Embankments on Pile-Similar Elements. In Proceedings of the EuroGeo3, Munich, Germany, 1–4 March 2004; pp. 279–284.
32. Van Eekelen, S.J.M.; Bezuijen, A.; Van Tol, A.F. An Analytical Model for Arching in Piled Embankments. *Geotext. Geomembr.* **2013**, *39*, 78–102. [CrossRef]
33. Van Eekelen, S.J.M.; Bezuijen, A.; Van Tol, A.F. Validation of Analytical Models for the Design of Basal Reinforced Piled Embankments. *Geotext. Geomembr.* **2015**, *43*, 56–81. [CrossRef]
34. Rui, R.; Van Tol, F.; Xia, X.-L.; Van Eekelen, S.; Hu, G.; Xia, Y. Evolution of Soil Arching; 2D DEM Simulations. *Comput. Geotech.* **2016**, *73*, 199–209. [CrossRef]
35. Zhang, Z.; Tao, F.; Han, J.; Ye, G.; Cheng, B.; Liu, L. Influence of Surface Footing Loading on Soil Arching above Multiple Buried Structures in Transparent Sand. *Can. J. Civ. Eng.* **2021**, *48*, 124–133. [CrossRef]
36. Zhang, Z.; Tao, F.-J.; Han, J.; Ye, G.-B.; Cheng, B.-N.; Xu, C. Arching Development in Transparent Soil during Multiple Trapdoor Movement and Surface Footing Loading. *Int. J. Geomech.* **2021**, *21*, 04020262. [CrossRef]
37. Hong, W.P.; Lee, J.H.; Lee, K.W. Load Transfer by Soil Arching in Pile-Supported Embankments. *Soils Found.* **2007**, *47*, 833–843. [CrossRef]

38. Wang, T.; Nguyen, V.D.; Bui, P.D.; Luo, Q.; Liu, K.; Zhang, L. Three-Dimensional Physical Modeling of Load Transfer in Basal Reinforced Embankments under Differential Settlement. *Geotext. Geomembr.* **2023**, *51*, 330–341. [CrossRef]
39. Chevalier, B.; Combe, G.; Villard, P. Experimental and Discrete Element Modeling Studies of the Trapdoor Problem: Influence of the Macro-Mechanical Frictional Parameters. *Acta Geotech.* **2012**, *7*, 15–39. [CrossRef]
40. Jenck, O.; Combe, G.; Emeriault, F.; De Pasquale, A. Arching Effect in a Granular Soil Subjected to Monotonic or Cyclic Loading: Kinematic Analysis. In Proceedings of the ICPMG2014—Physical Modelling in Geotechnics, Perth, Australia, 14–17 January 2014; Gaudin, C., White, D., Eds.; CRC Press: Boca Raton, FL, USA, 2014; pp. 1243–1249, ISBN 978-1-138-00152-7.
41. Xu, C.; Zhang, X.; Han, J.; Yang, Y. Two-Dimensional Soil-Arching Behavior under Static and Cyclic Loading. *Int. J. Geomech.* **2019**, *19*, 04019091. [CrossRef]
42. Al-Naddaf, M.; Han, J.; Xu, C.; Jawad, S.; Abdulrasool, G. Experimental Investigation of Soil Arching Mobilization and Degradation under Localized Surface Loading. *J. Geotech. Geoenviron. Eng.* **2019**, *145*, 04019114. [CrossRef]
43. Al-Naddaf, M.; Han, J. Spring-Based Trapdoor Tests Investigating Soil Arching Stability in Embankment Fill under Localized Surface Loading. *J. Geotech. Geoenviron. Eng.* **2021**, *147*, 04021087. [CrossRef]
44. Naughton, P.J.; Kempton, G.T. Comparison of Analytical and Numerical Analysis Design Methods for Piled Embankments. In Proceedings of the Contemporary Issues in Foundation Engineering, Austin, TX, USA, 24–26 January 2005; American Society of Civil Engineers: Reston, VA, USA, 2005; pp. 1–10.
45. Van Eekelen, S.J.M.; Van, M.A.; Bezuijen, A. The Kyoto Road, a Full-Scale Test. Measurements and Calculations. In Proceedings of the 14th European Conference on Soil Mechanics and Geotechnical Engineering, Madrid, Spain, 24–27 September 2007; pp. 1533–1538.
46. Abusharar, S.W.; Zheng, J.-J.; Chen, B.-G.; Yin, J.-H. A Simplified Method for Analysis of a Piled Embankment Reinforced with Geosynthetics. *Geotext. Geomembr.* **2009**, *27*, 39–52. [CrossRef]
47. Al-Ani, W.; Wanatowski, D.; Chan, S.H. Numerical Analysis of Piled Embankments on Soft Soils. In Proceedings of the Ground Improvement and Geosynthetics, Shanghai, China, 26–28 May 2014; American Society of Civil Engineers: Reston, VA, USA, 2014; pp. 30–39.
48. Zhuang, Y.; Wang, K.Y. Finite-Element Analysis on the Effect of Subsoil in Reinforced Piled Embankments and Comparison with Theoretical Method Predictions. *Int. J. Geomech.* **2016**, *16*, 04016011. [CrossRef]
49. Wang, H.-L.; Chen, R.-P. Estimating Static and Dynamic Stresses in Geosynthetic-Reinforced Pile-Supported Track-Bed under Train Moving Loads. *J. Geotech. Geoenviron. Eng.* **2019**, *145*, 04019029. [CrossRef]
50. Van Eekelen, S.J.M.; Bezuijen, A.; Van Tol, A.F. Analysis and Modification of the British Standard BS8006 for the Design of Piled Embankments. *Geotext. Geomembr.* **2011**, *29*, 345–359. [CrossRef]
51. Zhuang, Y.; Wang, K.Y.; Liu, H.L. A Simplified Model to Analyze the Reinforced Piled Embankments. *Geotext. Geomembr.* **2014**, *42*, 154–165. [CrossRef]
52. Pham, T.A. Analysis of Geosynthetic-Reinforced Pile-Supported Embankment with Soil-Structure Interaction Models. *Comput. Geotech.* **2020**, *121*, 103438. [CrossRef]
53. Pham, T.A. Load-Deformation of Piled Embankments Considering Geosynthetic Membrane Effect and Interface Friction. *Geosynth. Int.* **2020**, *27*, 275–300. [CrossRef]
54. Pham, T.A.; Wijesuriya, K.; Dias, D. Analytical Model for the Design of Piled Embankments Considering Cohesive Soils. *Geosynth. Int.* **2022**, *29*, 369–388. [CrossRef]
55. Chen, Y.-M.; Cao, W.-P.; Chen, R.-P. An Experimental Investigation of Soil Arching within Basal Reinforced and Unreinforced Piled Embankments. *Geotext. Geomembr.* **2008**, *26*, 164–174. [CrossRef]
56. Han, J.; Gabr, M.A. Numerical Analysis of Geosynthetic-Reinforced and Pile-Supported Earth Platforms over Soft Soil. *J. Geotech. Geoenviron. Eng.* **2002**, *128*, 44–53. [CrossRef]
57. Murugesan, S.; Rajagopal, K. Geosynthetic-Encased Stone Columns: Numerical Evaluation. *Geotext. Geomembr.* **2006**, *24*, 349–358. [CrossRef]
58. Nguyen, V.D.; Luo, Q.; Xue, Y.; Wang, T.; Zhang, L.; Zhang, D. Extended Concentric Arches Model for Piled Beam-Supported Embankments. *Comput. Geotech.* **2023**, *160*, 105517. [CrossRef]
59. Wang, T.; Ma, H.; Liu, K.; Luo, Q.; Xiao, S. Load Transfer and Performance Evaluation of Piled Beam-Supported Embankments. *Acta Geotech.* **2022**, *17*, 4145–4171. [CrossRef]
60. Wang, G.; Zhang, X.; Liu, X.; Wang, H.; Xu, L.; Liu, H.; Peng, L. Soil Arching Effect in Reinforced Piled Embankment for Motor-Racing Circuit: Field Tests and Numerical Analysis. *Transp. Geotech.* **2022**, *37*, 100844. [CrossRef]
61. Rowe, R.K.; Liu, K.-W. Three-Dimensional Finite Element Modelling of a Full-Scale Geosynthetic-Reinforced, Pile-Supported Embankment. *Can. Geotech. J.* **2015**, *52*, 2041–2054. [CrossRef]
62. Van Eekelen, S.J.M.; Bezuijen, A.; Lodder, H.J.; Van Tol, A.F. Model Experiments on Piled Embankments. Part I. *Geotext. Geomembr.* **2012**, *32*, 69–81. [CrossRef]
63. Van Eekelen, S.J.M.; Bezuijen, A.; Lodder, H.J.; Van Tol, A.F. Model Experiments on Piled Embankments. Part II. *Geotext. Geomembr.* **2012**, *32*, 82–94. [CrossRef]

64. Ye, X.; Wu, J.; Li, G. Time-Dependent Field Performance of PHC Pile-Cap-Beam-Supported Embankment over Soft Marine Clay. *Transp. Geotech.* **2021**, *26*, 100435. [CrossRef]
65. Zhuang, Y.; Wang, K. Finite Element Analysis on the Dynamic Behavior of Soil Arching Effect in Piled Embankment. *Transp. Geotech.* **2018**, *14*, 8–21. [CrossRef]
66. Zheng, G.; Yang, X.; Zhou, H.; Chai, J. Numerical Modeling of Progressive Failure of Rigid Piles under Embankment Load. *Can. Geotech. J.* **2019**, *56*, 23–34. [CrossRef]
67. Ma, H.; Luo, Q.; Wang, T.; Jiang, H.; Lu, Q. Numerical Stability Analysis of Piled Embankments Reinforced with Ground Beams. *Transp. Geotech.* **2021**, *26*, 100427. [CrossRef]
68. Hosseinpour, I.; Riccio, M.; Almeida, M.S.S. Numerical Evaluation of a Granular Column Reinforced by Geosynthetics Using Encasement and Laminated Disks. *Geotext. Geomembr.* **2014**, *42*, 363–373. [CrossRef]
69. Hosseinpour, I.; Almeida, M.S.S.; Riccio, M. Full-Scale Load Test and Finite-Element Analysis of Soft Ground Improved by Geotextile-Encased Granular Columns. *Geosynth. Int.* **2015**, *22*, 428–438. [CrossRef]
70. Zhang, C.; Su, L.; Jiang, G. Full-Scale Model Tests of Load Transfer in Geogrid-Reinforced and Floating Pile-Supported Embankments. *Geotext. Geomembr.* **2022**, *50*, 896–909. [CrossRef]
71. Pan, G.; Liu, X.; Yuan, S.; Wang, Y.; Sun, D.; Feng, Y.; Jiang, G. A Field Study on the Arching Behavior of a Geogrid-Reinforced Floating Pile-Supported Embankment. *Transp. Geotech.* **2022**, *37*, 100795. [CrossRef]
72. Zhuang, Y.; Wang, K.Y. Finite-Element Analysis of Arching in Highway Piled Embankments Subjected to Moving Vehicle Loads. *Géotechnique* **2018**, *68*, 857–868. [CrossRef]
73. Qin, C.; Hazarika, H.; Pasha, S.M.K.; Furuichi, H.; Kochi, Y.; Matsumoto, D.; Fujishiro, T.; Ishibashi, S.; Watanabe, N.; Yamamoto, S. Evaluation of Hybrid Pile Supported System for Protecting Road Embankment Under Seismic Loading. In *Advances in Sustainable Construction and Resource Management*; Hazarika, H., Madabhushi, G.S.P., Yasuhara, K., Bergado, D.T., Eds.; Lecture Notes in Civil Engineering; Springer: Singapore, 2021; Volume 144, pp. 733–744, ISBN 9789811600760.
74. Chen, Y.; Ma, S.; Ren, Y.; Chen, R.; Bian, X. Experimental Study on Cyclic Settlement of Piles in Silt Soil and Its Application in High-Speed Railway Design. *Transp. Geotech.* **2021**, *27*, 100496. [CrossRef]
75. Qin, C.; Hazarika, H.; Rohit, D.; Ogawa, N.; Kochi, Y.; Liu, G. *Numerical Simulation of Seismic Performance of Road Embankment Improved with Hybrid Type Steel Pile Reinforcement*; Springer: Beijing, China, 2022; pp. 1332–1339.
76. Lai, H.-J.; Zheng, J.-J.; Zhang, J.; Zhang, R.-J.; Cui, L. DEM Analysis of "Soil"-Arching within Geogrid-Reinforced and Unreinforced Pile-Supported Embankments. *Comput. Geotech.* **2014**, *61*, 13–23. [CrossRef]
77. Lai, H.-J.; Zhang, J.-J.; Zhang, R.-J.; Cui, M.-J. Visualization of the Formation and Features of Soil Arching within a Piled Embankment by Discrete Element Method Simulation. *J. Zhejiang Univ.-Sci. Appl. Phys. Eng.* **2016**, *17*, 803–817. [CrossRef]
78. Lai, H.-J.; Zheng, J.-J.; Zhang, R.-J.; Cui, M.-J. Classification and Characteristics of Soil Arching Structures in Pile-Supported Embankments. *Comput. Geotech.* **2018**, *98*, 153–171. [CrossRef]
79. Lai, H.-J.; Zheng, J.-J.; Cui, M.-J.; Chu, J. "Soil Arching" for Piled Embankments: Insights from Stress Redistribution Behaviour of DEM Modelling. *Acta Geotech.* **2020**, *15*, 2117–2136. [CrossRef]
80. Papamichos, E.; Vardoulakis, I.; Heil, L.K. Overburden Modeling above a Compacting Reservoir Using a Trap Door Apparatus. *Phys. Chem. Earth Part Solid Earth Geod.* **2001**, *26*, 69–74. [CrossRef]
81. Van Eekelen, S.J.M.; Bezuijen, A.; Oung, O. Arching in Piled Embankments; Experiments and Design Calculations. In *BGA International Conference on Foundations: Innovations, Observations, Design and Practice, Proceedings of the International Conference Organised by British Geotechnical Association and Held in Dundee, Scotland on 2–5 September 2003*; Thomas Telford Publishing: London, UK, 2003; pp. 885–894.
82. Shahin, H.M.; Nakai, T.; Hinokio, M.; Kurimoto, T.; Sada, T. Influence of Surface Loads and Construction Sequence on Ground Response Due to Tunnelling. *Soils Found.* **2004**, *44*, 71–84. [CrossRef]
83. Rui, R.; Van Tol, A.F.; Xia, Y.Y.; Van Eekelen, S.J.M.; Hu, G. Investigation of Soil-Arching Development in Dense Sand by 2D Model Tests. *Geotech. Test. J.* **2016**, *39*, 20150130. [CrossRef]
84. Rui, R.; Han, J.; Zhang, L.; Zhai, Y.; Cheng, Z.; Chen, C. Simplified Method for Estimating Vertical Stress-Settlement Responses of Piled Embankments on Soft Soils. *Comput. Geotech.* **2020**, *119*, 103365. [CrossRef]
85. Rui, R.; Ye, Y.; Han, J.; Zhai, Y.; Wan, Y.; Chen, C.; Zhang, L. Two-Dimensional Soil Arching Evolution in Geosynthetic-Reinforced Pile-Supported Embankments over Voids. *Geotext. Geomembr.* **2022**, *50*, 82–98. [CrossRef]
86. Xu, C.; Song, S.; Han, J. Scaled Model Tests on Influence Factors of Full Geosynthetic-Reinforced Pile-Supported Embankments. *Geosynth. Int.* **2016**, *23*, 140–153. [CrossRef]
87. Chen, R.P.; Chen, Y.M.; Han, J.; Xu, Z.Z. A Theoretical Solution for Pile-Supported Embankments on Soft Soils under One-Dimensional Compression. *Can. Geotech. J.* **2008**, *45*, 611–623. [CrossRef]
88. Lee, T.; Van Eekelen, S.J.M.; Jung, Y.-H. Numerical Verification of the Concentric Arches Model for Geosynthetic-Reinforced Pile-Supported Embankments: Applicability and Limitations. *Can. Geotech. J.* **2021**, *58*, 441–454. [CrossRef]
89. Samira, F.; Larbi, M.; Mouloud, M.; Laurent, B. Subsoil Compressibility Effect in an End Bearing Scaled Pile-Supported Embankment, Investigation of the Load Transfer Mechanism. *Innov. Infrastruct. Solut.* **2022**, *7*, 75. [CrossRef]

90. Chen, R.P.; Xu, Z.Z.; Chen, Y.M.; Ling, D.S.; Zhu, B. Field Tests on Pile-Supported Embankments over Soft Ground. *J. Geotech. Geoenviron. Eng.* **2010**, *136*, 777–785. [CrossRef]
91. Esmaeili, M.; Khajehei, H. Mechanical Behavior of Embankments Overlying on Loose Subgrade Stabilized by Deep Mixed Columns. *J. Rock Mech. Geotech. Eng.* **2016**, *8*, 651–659. [CrossRef]
92. Rui, R.; Han, J.; Van Eekelen, S.J.M.; Wan, Y. Experimental Investigation of Soil-Arching Development in Unreinforced and Geosynthetic-Reinforced Pile-Supported Embankments. *J. Geotech. Geoenviron. Eng.* **2019**, *145*, 04018103. [CrossRef]
93. Zhang, C.; Jiang, G.; Liu, X.; Buzzi, O. Arching in Geogrid-Reinforced Pile-Supported Embankments over Silty Clay of Medium Compressibility: Field Data and Analytical Solution. *Comput. Geotech.* **2016**, *77*, 11–25. [CrossRef]
94. Lai, H.-J.; Zheng, J.-J.; Cui, M.-J. Improved Analytical Soil Arching Model for the Design of Piled Embankments. *Int. J. Geomech.* **2021**, *21*, 04020261. [CrossRef]
95. Zhang, Z.; Wang, M.; Ye, G.-B.; Han, J. A Novel 2D-3D Conversion Method for Calculating Maximum Strain of Geosynthetic Reinforcement in Pile-Supported Embankments. *Geotext. Geomembr.* **2019**, *47*, 336–351. [CrossRef]
96. Meena, N.K.; Nimbalkar, S.; Fatahi, B.; Yang, G. Effects of Soil Arching on Behavior of Pile-Supported Railway Embankment: 2D FEM Approach. *Comput. Geotech.* **2020**, *123*, 103601. [CrossRef]
97. Jones, B.M.; Plaut, R.H.; Filz, G.M. Analysis of Geosynthetic Reinforcement in Pile-Supported Embankments. Part I: 3D Plate Model. *Geosynth. Int.* **2010**, *17*, 59–67. [CrossRef]
98. Ye, G.-B.; Wang, M.; Zhang, Z.; Han, J.; Xu, C. Geosynthetic-Reinforced Pile-Supported Embankments with Caps in a Triangular Pattern over Soft Clay. *Geotext. Geomembr.* **2020**, *48*, 52–61. [CrossRef]
99. Wijerathna, M.; Liyanapathirana, D.S. Load Transfer Mechanism in Geosynthetic Reinforced Column-Supported Embankments. *Geosynth. Int.* **2020**, *27*, 236–248. [CrossRef]
100. Le Hello, B.; Villard, P. Embankments Reinforced by Piles and Geosynthetics—Numerical and Experimental Studies Dealing with the Transfer of Load on the Soil Embankment. *Eng. Geol.* **2009**, *106*, 78–91. [CrossRef]
101. Fagundes, D.F.; Almeida, M.S.S.; Thorel, L.; Blanc, M. Load Transfer Mechanism and Deformation of Reinforced Piled Embankments. *Geotext. Geomembr.* **2017**, *45*, 1–10. [CrossRef]
102. Pham, T.A.; Dias, D. 3D Numerical Study of the Performance of Geosynthetic-Reinforced and Pile-Supported Embankments. *Soils Found.* **2021**, *61*, 1319–1342. [CrossRef]
103. Bhasi, A.; Rajagopal, K. Numerical Investigation of Time Dependent Behavior of Geosynthetic Reinforced Piled Embankments. *Int. J. Geotech. Eng.* **2013**, *7*, 232–240. [CrossRef]
104. Eskişar, T.; Otani, J.; Hironaka, J. Visualization of Soil Arching on Reinforced Embankment with Rigid Pile Foundation Using X-Ray CT. *Geotext. Geomembr.* **2012**, *32*, 44–54. [CrossRef]
105. Jenck, O.; Dias, D.; Kastner, R. Two-Dimensional Physical and Numerical Modeling of a Pile-Supported Earth Platform over Soft Soil. *J. Geotech. Geoenviron. Eng.* **2007**, *133*, 295–305. [CrossRef]
106. Chen, C.-Y.; Martin, G.R. Soil–Structure Interaction for Landslide Stabilizing Piles. *Comput. Geotech.* **2002**, *29*, 363–386. [CrossRef]
107. Borges, J.L.; Marques, D.O. Geosynthetic-Reinforced and Jet Grout Column-Supported Embankments on Soft Soils: Numerical Analysis and Parametric Study. *Comput. Geotech.* **2011**, *38*, 883–896. [CrossRef]
108. Zhang, X.; Zhuang, Y.; Hu, S.; Dong, X. A Simplified Method for Assessing the Serviceability Performance of Geosynthetic Reinforced and Pile-Supported Embankment. *Geotext. Geomembr.* **2022**, *50*, 1214–1229. [CrossRef]
109. Arulrajah, A.; Abdullah, A.; Bo, M.W.; Bouazza, A. Ground Improvement Techniques for Railway Embankments. *Proc. Inst. Civ. Eng.—Ground Improv.* **2009**, *162*, 3–14. [CrossRef]
110. Arulrajah, A.; Abdullah, A.; Bo, M.W.; Leong, M. Geosynthetic Applications in High-Speed Railways: A Case Study. *Proc. Inst. Civ. Eng.—Ground Improv.* **2015**, *168*, 3–13. [CrossRef]
111. Zhuang, Y.; Cheng, X.; Wang, K. Analytical Solution for Geogrid-Reinforced Piled Embankments under Traffic Loads. *Geosynth. Int.* **2020**, *27*, 249–260. [CrossRef]
112. Bhasi, A.; Rajagopal, K. Geosynthetic-Reinforced Piled Embankments: Comparison of Numerical and Analytical Methods. *Int. J. Geomech.* **2015**, *15*, 04014074. [CrossRef]
113. Zhuang, Y.; Wang, K.Y. Three-Dimensional Behavior of Biaxial Geogrid in a Piled Embankment: Numerical Investigation. *Can. Geotech. J.* **2015**, *52*, 1629–1635. [CrossRef]
114. Xu, C.; Wu, D.; Song, S.; Liu, B. Centrifuge Model Tests of Basal Reinforcement Effects on Geosynthetic-Reinforced Pile-Supported Embankment. In Proceedings of the GeoShanghai 2018 International Conference: Ground Improvement and Geosynthetics, Shanghai, China, 27–30 May 2018; Li, L., Cetin, B., Yang, X., Eds.; Springer: Singapore, 2018; pp. 279–287, ISBN 9789811301216.
115. Shen, P.; Xu, C.; Han, J. Centrifuge Tests to Investigate Global Performance of Geosynthetic-Reinforced Pile-Supported Embankments with Side Slopes. *Geotext. Geomembr.* **2020**, *48*, 120–127. [CrossRef]
116. Badakhshan, E.; Noorzad, A.; Bouazza, A.; Zameni, S.; King, L. A 3D-DEM Investigation of the Mechanism of Arching within Geosynthetic-Reinforced Piled Embankment. *Int. J. Solids Struct.* **2020**, *187*, 58–74. [CrossRef]
117. Cao, W.Z.; Zheng, J.J.; Zhang, J.; Zhang, R.J. Field Test of a Geogrid-Reinforced and Floating Pile-Supported Embankment. *Geosynth. Int.* **2016**, *23*, 348–361. [CrossRef]

118. Li, G.; Xu, C.; Yoo, C.; Shen, P.; Wang, T.; Zhao, C. Effect of Geogrid Reinforcement on the Load Transfer in Pile-Supported Embankment under Cyclic Loading. *Geotext. Geomembr.* **2023**, *51*, 151–164. [CrossRef]
119. Shen, P.; Xu, C.; Han, J. Geosynthetic-Reinforced Pile-Supported Embankment: Settlement in Different Pile Conditions. *Geosynth. Int.* **2020**, *27*, 315–331. [CrossRef]